Kinematics of the Suez-Sinai area from combined GPS velocity field

G. Pietrantonio[1], R. Devoti[1], S. Mahmoud[2], F. Riguzzi[1]

[1] Istituto Nazionale di Geofisica e Vulcanologia, sez. CNT, Roma, Italy

[2] National Research Institute of Astronomy and Geophysics, Cairo, Egypt

Abstract

A combined GPS velocity solution covering a wide area from Egypt to Middle East allowed us to infer the current rates across the main, already well known, tectonic features. We have estimated 126 velocities from time series of 90 permanent and 36 non permanent GPS sites located in Africa (Egypt), Eurasia and Arabia plates in the time span 1996-2015, the largest available for the Egyptian sites. We have combined our velocity solution in a least-squares sense with two other recent velocity solutions of networks located around the eastern Mediterranean, obtaining a final IGb08 velocity field of about 450 sites. Then, we have estimated the IGb08 Euler poles of Africa, Sinai and Arabia, analyzing the kinematics of the Sinai area, particular velocity profiles, and estimating the 2D strain rate field. We show that it is possible to reliably model the rigid motion of Sinai block only including some GPS sites located south of the Carmel Fault. The estimated relative motion with respect to Africa is of the order of 2-3 mm/yr, however there is a clear mismatch between the modeled and the observed velocities in the southern Sinai sites. We have also assessed the NNE left shear motion along the Dead Sea Transform Fault, estimating a relative motion between Arabia and Africa of about 6 mm/yr in the direction of the Red Sea opening.

Keywords: Africa, Arabia, Sinai, Gulf of Aqaba, Gulf of Suez, GPS, combined velocity field, Euler poles

Introduction

Egypt is located in the Eastern Mediterranean, at the north-eastern corner of the African continent, a region dominated by the relative motion of 3 major plates. The subduction between African and Eurasian plates and the opening of the Red Sea represent the boundaries between African, Arabian and Eurasian plates.

Sinai peninsula is located north of the triple junction among the Gulf of Suez rift, the Aqaba-Levant transform fault (the southernmost part of the Dead Sea Fault System) and the Red Sea rift (Ben-Menahem et al., 1976); from a geodynamic point of view it is generally considered as an independent sub-plate of the African plate interacting with the Arabian and Eurasian plates (Saleh and Becker, 2015 and references therein).

In the last decades, many geological and seismological investigations were developed in this area, especially for petroleum researches so that the tectonic history is well known (e.g. Lindquist, 1998). From early to late Miocene, the area was subjected to different phases of motion. At the beginning the northeastward motion of the Arabian peninsula yielded the opening of the Red Sea; subsequently, the rifting propagated toward NW, along the Gulf of Suez area. The rifting is thought to culminate in early-middle Miocene when the stresses of the Red Sea rift were transferred along the Aqaba-Levant area generating a left-lateral transform fault that extends through the Gulf of Aqaba northeastward to the Dead Sea, with a minor extensional component (Steckler et al., 1988, Le Pichon et al., 1988). The question of whether the triggered motion of the Aqaba-Levant fault system has entirely or partially replaced the Gulf of Suez opening is not completely solved. The present day tectonic activity of the area is testified by an ongoing seismic activity generally characterized by small to moderate earthquakes due to the relative motions between the African, Arabian and Eurasian plates. There are three main seismic zones: the Northern Red Sea, Gulf of Suez and Gulf of Aqaba. The highest seismicity rates are detected at the eastern boundaries along the Gulf of Aqaba and the northern part of the Red Sea. Moderate seismicity is also present in the Cairo area. Studies demonstrate mainly a normal faulting mechanism with minor strike slip component generally trending parallel to the northern Red Sea, the Suez rift, Aqaba rift with their

connection with the great rift system of the Red Sea and the Gulf of Suez and Cairo-Alexandria trend (Emad Mohamed et al., 2015).

Many studies based on GPS data, have been carried out to shed light on the current kinematics of this key area. Earlier studies based on very few GPS observations attempted to estimate the motion of the Sinai area from repeated surveys (Riguzzi et al.,1999) and elastic block model (Mahmoud et al., 2005) defining Sinai as a separate sub-plate sandwiched between the Arabian and African plates. Piersanti et al. (2001) and Riguzzi et al. (2006) found short-term deformations from GPS survey data in the Sinai area and speculated about the possible role of post-seismic relaxation. Other studies based on wider datasets, but including few GPS stations in the Egypt-Sinai region, estimated the Euler vectors of the relative motion of the Africa, Arabian and Eurasian plates (McClusky et al., 2003; Reilinger et al., 2006) and the crustal deformation due to the ongoing active processes along the Dead Sea Fault System (Le Beon et al., 2008; Sadeh et al., 2012; Palano et al., 2013).

Recently, Saleh and Becker (2015) have included in their study GPS data of permanent and non permanent stations in Egypt covering the period 2006-2012, assessing velocity and strain rate fields and estimating the relative motion between African, Eurasian and Arabian plates; they have detected no significant differential motion between Sinai and Africa.

In this paper, in order to assess more details on the kinematics of the Suez Gulf-Sinai area and the current rates across the main tectonic features of this region, we have used the largest data set, including 16 Egyptian permanent sites, many other permanent sites located in Eurasia, Africa and Arabia plates and including campaign data from Egyptian networks surveyed during the period 1996-2005.

We have homogeneously reprocessed by the Bernese software all these data (permanent and non permanent) covering a total time span of 20 years. Then, we have combined our IGb08 (IGS realization of the ITRF2008) velocity solution with the solution of Saleh and Becker (2015) and with a velocity subset of the global solution published by Kreemer et al. (2014), obtaining a final IGb08 velocity field of 457 sites in our study area.

GPS data and processing steps

The National Research Institute for Astronomy and Geophysics (NRIAG) established different GPS networks around active areas in Egypt, starting in 1996 in the Greater Cairo region. Subsequently, several other non permanent sites were installed in the Aswan region, Sinai peninsula, Gulf of Suez, Nile Valley (Saleh and Becker, 2015; Riguzzi et al., 2006). Finally, in 2006 NRIAG started the construction of a permanent GPS network in Egypt (EPGN – Egyptian Permanent GPS Network), consisting at present of 16 stations (Saleh and Becker, 2013).

We have collected data of 16 permanent and 36 non permanent sites in Egypt in the time span 1996-2015; in particular the GPS campaigns cover the interval 1996-2005, while continuous sites span from the end of 2006 to the middle of 2015. In addition, we have included in our processing IGS sites in the surrounding regions, in Africa, Europe, Arabia and Israel and some other permanent stations archived at SOPAC and UNAVCO (see Figures S1, S2, S3 in the supplementary material).

Our analysis follows a procedure that can be summarized in 4 main steps: *1)* daily processing of GPS data, *2)* combination of daily solutions and reference frame definition, *3)* time series analysis and velocity field estimation, *4)* combination of our velocity field with other two different solutions.

1. *Daily processing of GPS data*

We have processed the GPS data by Bernese GNSS software 5.0 (Dach et al., 2007), following the Guidelines for EUREF Analysis Centers (http://www.epncb.oma.be).

We have fixed the GPS orbits and Earth's orientation parameters to the combined IGS products and assigned an a priori loose constraint of 10 m to all the site coordinates. We have applied the elevation-dependent phase center corrections and the absolute phase center calibrations. The troposphere modeling consists in an a priori dry-Niell model fulfilled by the estimation of zenith delay corrections at 1-hour intervals at each site using the wet-Niell mapping function; in addition one horizontal gradient parameter per day at each site is estimated. The ionosphere is not modeled a priori, but it is removed by applying the ionosphere-free linear combination of L1 and L2 carriers.

The ambiguity resolution is based on the QIF baseline-wise analysis. The final network solution is solved with back-substituted ambiguities, if integer, otherwise real ambiguities are considered measurement biases.

Thehe daily GPS solutions are not estimated in a given a priori reference frame but computed in a loosely constrained reference frame, applying loose a priori constraints (10 m) to all station coordinates. As a consequence, the positions are randomly translated or rotated from day-to-day and their covariance matrices have large errors (on the order of centimeters).

2. *Combination of daily solutions and reference frame definition*

Then, we have merged the daily "loose" solutions day by day with the daily loose solutions of a global network of about 60 IGS stations. Basically, the two sets of solutions share 9 common sites allowing the combination into a unique network solution by a classical least-squares approach (Devoti, 2012).

After these combinations, we have performed two main transformations to express the daily coordinates of the overall network in a unique reference frame and to compute the real covariance matrix. First the loose covariance matrix has been projected into the space of errors (Blewitt et al., 1992) imposing tight internal constraints (at the millimeter level), then the coordinates have been transformed into the IGb08 (Altamimi et al., 2012) by a 4-parameter Helmert transformation (3 translations and a scale factor) where the proper set of constraints is driven by the rank deficiency of the normal matrices. A comprehensive discussion of the rank deficiency of our solutions is given in Devoti et al. (2010).

3. *Time series analysis and velocity field estimation*

The site velocities have been estimated fitting simultaneously a linear drift, episodic offsets and annual sinusoids to all the coordinate time series. Offsets are estimated whenever a change in the GPS equipment induces a significant step in the time series, whereas seasonal oscillations are accounted by annual sinusoids. Data are rejected as outliers whenever the weighted residual exceeds three times the global chi square (χ^2). Finally, the formal errors have been scaled taking into account

the noise content of site daily time series, modeled as a combination of white and flicker noise, as described in Mao et al. (1999). At the end we obtained a full 3D velocity solution of 126 stations in the Egyptian and Middle-East region.

4. Combination of velocity fields

At this stage we have combined our velocity solution with two already available velocity solutions related to the same area (Saleh and Becker, 2015; Kreemer et al., 2014). Since the latter solutions concern only the horizontal components, in our combination we neglected the vertical rates. Figure 1 shows the three velocity fields, used as input for the combination adjustment, in a fixed Eurasian plate reference frame (Altamimi et al., 2012). About the velocity field of Saleh and Becker (2015), we have found an inconsistency in their published velocity values: there is a mismatch between their ITRF2008 velocity field (Table 1A in the Appendix of their paper) and the Eurasian fixed velocity field of their Table 5 and Figure 10, in fact from the first it is not possible to retrieve the second after removing the Eurasia motion of their Table 4. After some trials, we have assumed correct the velocity values reported in Table 1A of Saleh and Becker (2015).

After such clarification, the final step is our velocity combination procedure which is based on a linear least-squares approach (Devoti et al., 2010; Devoti, 2012). We consider each velocity field as a sample of the true velocity field and the combined velocity as the best estimate of the true velocity field. The combined solution allows a validation of the velocity field by assessing the velocity repeatability of the common sites and reduces to a minimum the chance of including biased velocities.

A major problem in combining individual velocity solutions is the recognition of station identity, since different authors generally adopt different naming conventions. We have used an approach based on the assignment of a unique label based on the station positions (geo-coding), in particular we have chosen the GHAM code proposed by Agnew (2005) to label each GPS station unambiguously. We have chosen a 12-character code providing a tag to geographic locations with a

cell size of 1.9 m (square root of area), sufficiently small to identify a single GPS antenna installation.

Multiple velocities, referring to the same station (same geo-code) have been estimated as tied velocities, using the classical method of Lagrange multipliers (e.g. Arfken et al., 2013), where the least squares are solved with the constraints of having equal velocities.

The normal matrix is formed from the three individual velocity solutions, and then it is inverted to estimate the unified velocity field of the entire network. As the covariance matrix is usually known apart from a constant multiplier, and in order to balance the relative weights of the input solutions, the combination is iterated 2 times in order to estimate a solution weighting factor based on each solution χ^2. The combined velocity field represents the weighted average of horizontal velocities taking into account the correlation matrices of the three solutions. The complete IGb08 combined velocity field is reported in Table S1 of the supplementary material. Figure 2 shows the histograms of the residuals of the three solutions with respect to the combined one, separately for the North and East components; only GPS sites with at least two different velocity solutions have been taken into account.

Combined velocity and strain rate fields

Our combined velocity field (Table S1 of the supplementary material), is more detailed with respect to those previously published, particularly at both sides of the Dead Sea Fault, permitting a better definition of the kinematics of the area.

We have estimated the Euler pole parameters for Africa, Arabia and Sinai from our IGb08 velocities, by selecting some GPS sites well representing the motion of the respective plates, far from highly deforming zones (Table 1).

The Sinai Euler pole turns out to be rather well estimated: Figure 3 shows the residual velocities with respect to this pole (in black the sites selected for pole estimation); the weighted mean of the

2D residuals is 0.4 mm/yr, the median of the North and East components are 0 and -0.05 mm/yr respectively.

	ω_X (°/Myr)	ω_Y (°/Myr)	ω_Z (°/Myr)	**Lat** (°)	**Lon** (°)	ω (°/Myr)
Africa	0.0389	-0.1654	0.2098	51.0	-76.8	0.270 ± 0.004
Sinai	0.2726	-0.0285	0.3661	53.2	-6.0	0.457 ± 0.023
Arabia	0.3186	-0.0532	0.3972	50.9	-9.5	0.512 ± 0.008

Table 1: Euler pole parameters of Africa, Sinai and Arabia estimated from IGb08 velocity solution

Figure 4 shows the combined GPS velocity field, expressed in the Africa-fixed reference frame (Table 1), neglecting the sites with at least one error ellipse semi-axis greater than 6 mm/yr. According to our rigid plate model, the Sinai block is rotating counterclockwise with respect to Africa with a pole of rotation located west of the Suez Canal (at 30.4°±0.8E, 30.0°±0.4N), indicated by a yellow star in Figure 4. The rigid block model predicts a general NNW trending motion, as highlighted by the dashed circles and the bold arrows, both in yellow Figure 4.

This model also predicts a decreasing extension rate from south (2.4 ± 0.3 mm/yr) to north (0.2 ± 0.3 mm/yr) along the Gulf of Suez (Figure 4, yellow symbols and black values in mm/yr). However, it is worth noting that the rigid plate model does not fit the southernmost Sinai velocities, both located along the Suez and Aqaba sides, with residuals as large as 2-3 mm/yr (Figure 3), thus emphasizing the weakness of rigid motion assumption near the triple junction area. The rigid plate model also predicts a significant, nearly constant, left-lateral strike-slip movement of about 1.0 ± 0.3 mm/yr along the Gulf of Suez (Figure 4, yellow symbols and black values in mm/yr).

In addition, the residual velocities with respect to the Sinai pole of Table 1 (Figure 3) indicate that the Carmel Fault System (CF) represents the boundary of Sinai block along its north-eastern corner, differently from Mahmoud et al., 2005, which established the Sinai block NE corner toward the Anatolian area. Indeed, our study shows that most of sites located north of CF have larger velocities than sites located south of it, in agreement with Sadeh et al. (2012).

In order to fully examine the existence of a separate Sinai sub-plate, we have also estimated the relative rotation pole of Arabia with respect to Africa; the relative motion is represented by the black dashed circular line in Figure 4. The Dead Sea Transform lies just along such great circle of the Arabian plate motion, from the triple junction south of the Sinai tip to the north of Dead Sea.

Further on, we have evaluated the horizontal strain rate as spatial gradient of the combined velocity field. We have used a distance-weighted approach, interpolating the GPS velocities on a regularly spaced grid, applying the weighting algorithm developed by Shen et al. (1996). Figure 5 shows the principal axes of the 2D strain rate tensor on a 0.5°x0.5° grid, superimposed to the so-called second invariant (accounting for all the 3 tensor components, $SI = \sqrt{\varepsilon_{11}^2 + \varepsilon_{22}^2 + 2\varepsilon_{12}^2}$) obtained by interpolating the velocity horizontal components on a 0.1°x0.1° regular grid. Strain rate values of 40-50·10^{-9}yr^{-1}, purely extensional, are reached in the Red Sea, being the extension orthogonal to the direction of Red Sea opening axis, and in the region of the Nile delta. The most deforming areas are located along the Dead Sea Transform Fault, where shear prevails, with values of the total strain rate up to 90·10^{-9}yr^{-1}. The areas of maximum deformation roughly coincide with those published in Saleh and Becker (2015), with values of the same order of magnitude. Instead our principal axis directions along the Dead Sea Transform Fault are turned by 90° with respect to those published in Saleh and Becker (2015) and are coherent with the well known left lateral shear style of this fault (Figure 5).

Results and discussion

Our velocity field is more detailed with respect to the previous published, particularly at both sides of the Dead Sea Fault, permitting a better definition of the kinematics of the area. The estimation of the Sinai-Africa relative Euler pole allows us to predict the rigid rotation of Sinai block with respect to Africa, represented by the yellow dashed circles and the yellow arrows in Figure 4. The observed velocities of the Sinai block, far from its boundaries, are coherent with the predicted ones. Exceptions are represented by the two sites along the south-western coast of Gulf of Aqaba and by

the site located at the tip of the peninsula (DAHA, NABQ, SHAM, see supplementary material); they are all non permanent sites. Since they are located in the proximity of the highly active Aqaba structure, we can argue that these sites are not representative of the rigid Sinai block motion, but are affected to same extent by inter-seismic elastic strain build-up near the pull-apart basins. On the contrary, GPS sites located along the Sinai coast of the Gulf of Suez show meaningless velocities always below 1-sigma level.

Our estimated relative Sinai-Africa pole is statistically compatible with the most recent published values of Saleh and Becker (2015) and also consistent with all geodetic solutions indicating a general extension across the Suez rift. Mahmoud et al. (2005) and Reilinger et al. (2006) using a block model approach evidenced an extension in the Gulf of Suez of 1-1.5 mm/yr which is also very close to our model, and reported a left lateral strike-slip motion of the order of 2 mm/yr that is higher but still close to our findings. Focal mechanisms obtained for a few earthquakes at the mouth of the Gulf of Suez show a predominant normal faulting component (McKenzie et al., 1970) but also argue in support of a left-lateral strike-slip faulting (Ben-Menahem et al., 1976; Huang and Solomon, 1987). The seismic data cited in support of these arguments include the largest earthquake occurred in the region (March 31, 1969, Ms=6.8), but also minor events that show focal mechanisms associated with shear mechanisms along the Suez rift (Emad Mohamed et al., 2015) and further north in correspondence of the Bitter Lakes, west of the Suez Canal (Salamon et al., 2003). Although the focal mechanisms suggest a complex relationship between the crustal deformation and the plate boundary, the kinematics of the Sinai block measured by GPS stations matches the main seismic slip directions observed in the area. Geological data indicate a post-Miocene total extension of about 30 km at the center of the Gulf (Joffe and Garfunkel, 1987; Steckler et al., 1998) that well agrees with our rigid plate model of 1.5 mm/yr (see Figure 4). In the northern part, the rift valley disappears showing a markedly decreasing extension, but small basins north of the Gulf, the Bitter Lakes and Lake Timsah, are arranged en-echelon, suggesting a small

strike-slip movement (Joffe and Garfunkel, 1987), in agreement with our estimated strike-slip motion model (~1 mm/yr).

Figure 4 also shows the rigid motion of Arabia with respect to Africa, represented by the black dashed circle. It's worth noting that the Dead Sea Transform Fault resembles such circle, from the triple junction south of the Sinai tip to the northern Dead Sea. This is in agreement with the fact that the Dead Sea Fault defines the plate boundary between Africa and Arabia, relieving the strain caused by the Red Sea rifting.

To highlight the inconsistencies between the rigid plate model and the GPS measurements, we have considered two velocity profiles (*a*, *b*, see Figure 6), involving sites on the three plates, crossing and being orthogonal to the Gulf of Suez and to the Dead Sea Transform direction respectively. We have considered the velocity projections, both parallel and orthogonal, to these two segments; the comparison between the parallel and perpendicular components evidences the extension vs shear motion components. The parallel component shows negligible extension rate across Gulf of Suez, as indicated by the strain rate principal axes of Figure 5. The perpendicular component shows evidence of the shear-rate along the Dead Sea Fault, confirming again the strain rate results of Figure 5; its trend is in agreement with a model of elastic loading on a locked dislocation that accommodates pure left-lateral shear at depth (e.g. Savage and Burford, 1973), as also reported in Le Beon et al. (2008) and Sadeh et al. (2012).

Moreover, we have considered a third velocity profile (*c*, see Figure 7), parallel to the Red Sea opening direction, crossing Sinai from Africa to Arabia. The velocities projection along this segment indicates that in this area the motion between Sinai and Africa appears insignificant, as we are considering the tip of Sinai where sites are not representative of the rigid block motion (Figure 4), as explained above. Highly active is the separation between Arabia and Sinai-Africa: by differencing the weighted average of velocity projections we have found a relative motion of about 6 mm/yr.

Conclusion

In this paper we have assessed details about the kinematics of a wide area covering Suez Gulf-Sinai region and surroundings by using the largest GPS data set available, including sites in Africa (Egypt), Sinai and Arabia. The velocity field has been derived by the combination of three individual velocity solutions, two of them recently published (Kreemer et al., 2014; Saleh and Becker, 2015) and the third obtained in the framework of this study by the Bernese software, analyzing permanent and non-permanent GPS data spanning 20 years.

The strain rate field, estimated by velocity interpolation on a regular grid, shows an extension rate of $40\text{-}50\cdot10^{-9}$ yr^{-1} in the Red Sea and in the region of Nile delta and the highest deformation along the Dead Sea Transform Fault, where shear prevails, with values of the total strain rate up to $90\cdot10^{-9}yr^{-1}$; the direction of principal strain rate axes are coherent with the direction of the Red Sea opening and with a left lateral shear zone along the Dead Sea Fault.

We have calculated the IGb08 Euler poles for Africa, Arabia and Sinai and the relative poles describing Sinai-Africa and Arabia-Africa motion.

Our results, both models and observations, emphasize the important shear rate acting along the Dead Sea Fault and a separation between Arabia and Sinai-Africa highly active, with a relative motion of about 6 mm/yr in the direction of the Red Sea opening.

Concerning the Sinai-Africa relative pole, the rigid plate motion model predicts a counterclockwise rotation of Sinai relative to Africa-fixed with tangential velocities of ~2 mm/yr. Such model predicts a small extension (from 0 to ~2 mm/yr moving from north to south) in the Gulf of Suez and a constant left-lateral strike-slip motion along the Gulf margin of ~1 mm/yr. We have to underline that the estimated Sinai rigid plate motion model indicates a significant misfit between the observed and the predicted velocities in the southern part of Sinai. In fact, the projected GPS velocities of Figure 6 and 7 show no extension in the Gulf of Suez area. However, a correct interpretation cannot disregard the fact that there are no permanent GPS stations in southern Sinai and that stations are close to the highly active Aqaba structure, affected by inter-seismic elastic strain build-up near the

pull-apart basins. To answer this question, it would be very useful to establish some permanent GPS site along the Sinai shore of Suez and Aqaba Gulfs.

Acknowledgements

We thank the staff members of NRIAG for providing GPS data of permanent stations and surveys. We are grateful to the individuals and institutions supporting the global IGS network, SOPAC and UNAVCO. We acknowledge the editor, the reviewer Guenter Stangl and another anonymous reviewer, their comments were very useful to improve the manuscript.

Supplementary material

Supplementary material associated with this article, consisting of three figures (Figures S1, S2, S3) and one table (Table S1), is provided in a separate file.

References

Agnew, D. C., 2005. GHAM: a compact global geocode suitable for sorting, Comput. Geosci., 31, 1042-1047, doi:10.1016/j.cageo.2005.02.007.

Altamimi, Z., Collilieux, X., Metivier, L., 2012. ITRF2008 Plate motion model, J. Geophys. Res., 117, B07402, doi:10.1029/2011JB008930.

Arfken, G.B., Weber, H.J., Harris, F.E., 2013. Mathematical Methods for Physicists, A comprehensive guide, 7th ed., Academic Press, Elsevier Inc., Oxford.

Ben-Menahem, A., Nur, A., Vered, M., 1976. Tectonics, seismicity and structure of the Afro-Eurasian junction - the breaking of an incoherent plate, Phys. Earth Planet. Int., 12, 1-50.

Bird, P., 2003. An updated digital model of plate boundaries, Geochem. Geophys. Geosyst., 4, 1027, doi:10.1029/2001GC000252.

Blewitt, G., Heflin, M.B., Webb, F. H., 1992. Global coordinates with centimeter accuracy in the International Terrestrial Reference Frame using GPS, Geophys. Res. Lett., 19 (9), 853-856.

Dach, R., Hugentobler, U., Fridez, P., Meindl, M. (Eds.), 2007. Bernese GPS Software Version 5.0. Manual. Astronomical Institute, University of Berne.

Devoti, R., Pietrantonio, G., Pisani, A.R., Riguzzi, F., Serpelloni, E., 2010. Present day kinematics of Italy. In: M. Beltrando, A. Peccerillo, M. Mattei, S. Conticelli & C. Doglioni (Eds), Journal of the Virtual Explorer, 36, 2.

Devoti R., 2012. Combination of coseismic displacement fields: a geodetic perspective, Annals of Geophysics, 55, 4, doi: 10.4401/ag-6119.

Emad Mohamed, K., Hassoup, A., Abou Elenean, K. M., Adel Othman, A. A., Diaa-Eldin Hamed, M. K., 2015. Earthquakes focal mechanism and stress field pattern in the northeastern part of Egypt, NRIAG Journal of Astronomy and Geophysics, 4, 205-221.

Huang, P.Y., Solomon, S.C., 1987. Centroid depths and mechanisms of mid-ocean ridge earthquakes in the Indian Ocean. Fulf of Aden, and Red Sea, J. Geophys. Res., 92, B2, 1361-1382.

Joffe, S., Garfunkel, Z., 1987. Plate kinematics of the circum Red Sea - a re-evaluation, Tectonophysics, 141, 5-22.

Kreemer, C., Blewitt, G., Klein, E.C., 2014. A geodetic plate motion and Global Strain Rate Model, Geochem. Geophys. Geosyst., 15, 3849–3889, doi:10.1002/2014GC005407.

Le Beon, M., Klinger, Y., Amrat, A.Q., Agnon, A., Dorbath, L., Baer, G., Ruegg, J.-C., Charade, O. Mayyas, O., 2008. Slip rate and locking depth from GPS profiles across the southern Dead Sea Transform, J. Geophys. Res., 113, B11403, doi:10.1029/2007JB005280.

Le Pichon, X., Gaulier, J.-M., 1988. The rotation of Arabia and the Levant fault system, Tectonophysics, 153, 271-294.

Lindquist, S.J., 1998. The Red Sea province: Sudr-Nubia and Maqna Petroleum Systems, Open File Report 99-50-A, USGS.

Mahmoud, S., Reilinger, R., McClusky, S., Vernant, P., Tealeb, A., 2005. GPS evidence for northward motion of the Sinai block: implications for E. Mediterranean tectonics, Earth Planet. Sci. Lett. 238, 217-224.

Mao, A., Harrison, C. G., & Dixon, T. H., 1999. Noise in GPS coordinate time series, J. Geophys. Res., 104(B2), 2797-2816.

McClusky, S., Reilinger, R., Mahmoud, S.M., Ben Sari, D., Tealeb, A., 2003. GPS constraints on Africa (Nubia) and Arabia plate motions, Geophys. J. Int. 155, 126–138.

McKenzie, D., Davies, D., Molnar, P., 1970. Plate tectonics of the Red Sea and East Africa, Nature, 226, 243-248.Palano, M., Imprescia, P., Gresta, S., 2013. Current stress and strain-rate fields across the Dead Sea Fault System: Constraints from seismological data and GPS observations, Earth Planet. Sci. Lett. 369-370, 305-316.

Piersanti, A., Nostro, C., Riguzzi, F., 2001. Active displacement field in the Suez–Sinai area: the role of post-seismic deformation, Earth Planet. Sci. Lett. 193, 13–23.

Reilinger, R., McClusky, S., Vernant, P., Lawrence, S., Ergintav, S., Cakmak, R., Ozener, H., Kadirov, F., Guliev, I., Stepanyan, R., Nadariya, M., Hahubia, G., Mahmoud, S., Sakr, K., ArRajehi, A., Paradissis, D., Al-Aydrus, A., Prilepin, M., Guseva, T., Evren, E., Dmitrotsa, A., Filikov, S.V., Gomez, F., Al-Ghazzi, R., Karam, G., 2006. GPS constraints on continental deformation in the Africa–Arabia–Eurasia continental collision zone and implications for the dynamics of plate interactions, J. Geophys. Res. 111, B05411, doi:10.1029/2005JB004051.

Riguzzi, F., Mahmoud, S., Tealeb, A., 1999. Displacement pattern of the Sinai area: first result from GPS, Annali di Geofisica 42 (4), 755–762.

Riguzzi, F., Pietrantonio, G., Piersanti, A., Mahmoud S.M., 2006. Current motion and short term deformations in the Suez-Sinai area from GPS observations, J. Geodyn., 41, 485-499.

Sadeh, M., Hamiel, Y., Ziv, A., Bock, Y., Fang, P., Wdowinski, S., 2012. Crustal deformation along the Dead Sea Transform and the Carmel Fault inferred from 12 years of GPS measurements, J. Geophys. Res., 117, B08410, doi:10.1029/2012JB009241.

Salamon, A., Hofstetter, A., Garfunkel, Z., Ron, H., 2003. Seismotectonics of the Sinai subplate - the eastern Mediterranean region, Geophys. J. Int., 155, 149-173.

Saleh, M., Becker, M., 2013. A new velocity field from the analysis of the Egyptian Permanent GPS Network (EPGN). Arab. J. Geosci., http://dx.doi.org/10.1007/s12517-013-1132-x.

Saleh, M., Becker, M., 2015. New constraints on the Nubia–Sinai–Dead Sea fault crustal motion, Tectonophysics, 651-652, 79-98.

Savage, J., Burford, R., 1973. Geodetic determination of relative plate motion in central California, J. Geophys. Res., 78, 832 – 845, doi:10.1029/JB078i005p00832.

Shen, Z.K., Jackson, D.D., Ge, B.X., 1996. Crustal deformation across and beyond the Los Angeles basin from geodetic measurements, J. Geophys. Res. 101, 27, 957-27, 980.

Steckler, M.S., Berthelot F., Liberis, N., Le Pichon, X., 1988. Subsidence in the Gulf of Suez: implications for rifting and plate kinematics, Tectonophysics, 153, 249-270.

Steckler, M.S., Feinstein, S., Kohn, B.P., Lavier, L.L., Eyal, M., 1998. Pattern of mantle thinning from subsidence and heat flow measurements in the Gulf of Suez: evidence for the rotation of Sinai and along-strike flow from the Red Sea, Tectonics, 17, 6, 903-920.

Figure Captions

Figure 1: The three velocity solutions, subsequently used as input for the combination, with respect to Eurasia fixed frame (Altamimi et al., 2012). In blue velocity subset from Kreemer et al. (2014); in green the solution from Saleh and Becker (2015); in red the solution obtained after this study. In the map some main tectonic features are schematically reported. The inset shows the plate boundaries of the 3 major plates Eurasia (EU), Africa (AF), Arabia (AR) and of Anatolian (AT) plate (Bird, 2003).

Figure 2: Horizontal velocity residuals (N, E) between each solution and the combined one, after a similarity transformation applied to the common sites; only sites with at least two different solutions are taken into account.

Figure 3: Residual velocities with respect to Sinai Euler pole; in black sites selected for pole estimation. CF indicates the Carmel Fault System, DST the Dead Sea Transform Fault System.

Figure 4: Combined velocity field with respect to the local Africa fixed frame (see Table 1). Yellow star and arrows tangent to yellow dashed circles indicate the pole of rotation and the rigid motion of Sinai block with respect to Africa, the scale of the yellow arrows is the same of the red arrows; yellow symbols along Gulf of Suez indicate the extension and shear rates (values in mm/yr) predicted by the rigid block model. Black dashed circular line represents the rigid motion of Arabia with respect to Africa.

Figure 5: Map of the strain rate obtained as spatial gradient of the combined horizontal velocity field. The colored background shows the so-called second invariant (accounting for all the 2D tensor components); the strain rate principal axes are also shown.

Figure 6: Velocities projected parallel and perpendicular to the lines *a* and *b* crossing the Suez and the Aqaba Gulfs (red lines in the inset) from Africa to Arabia. Below, the topography crossed by the lines.

Figure 7: Velocities projected along the line *c* (red line in the inset) crossing Sinai from Africa to Arabia, parallel to the Red Sea opening direction. Dashed lines are the weighted average of velocity projections. Below, the topography crossed by the line.

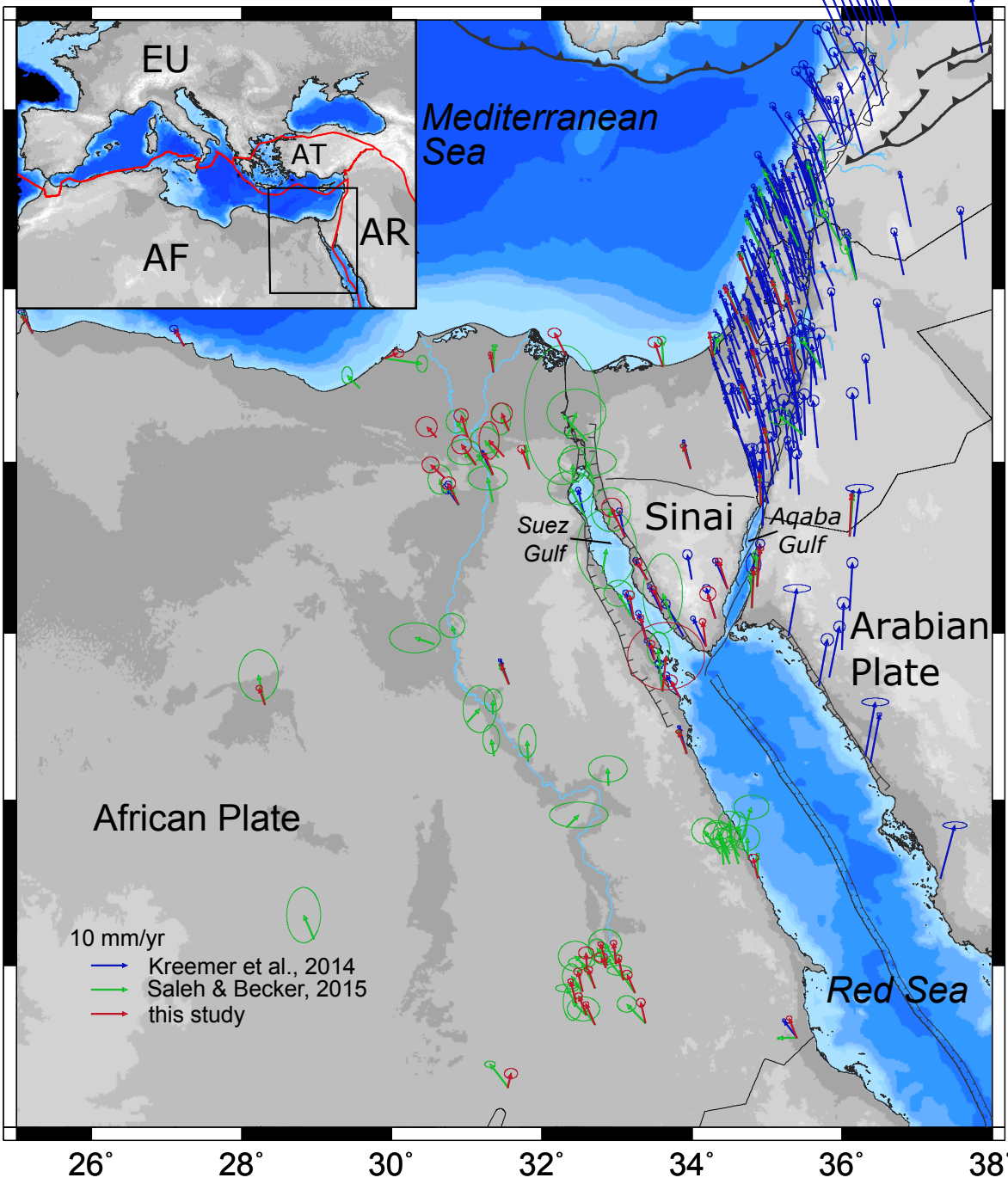
EU
AT
AR
AF
Mediterranean Sea
Sinai
Suez Gulf
Aqaba Gulf
Arabian Plate
African Plate
Red Sea
10 mm/yr
Kreemer et al., 2014
Saleh & Becker, 2015
this study
34˚
32˚
30˚
28˚
26˚
24˚
22˚
26˚
28˚
30˚
32˚
34˚
36˚
38˚

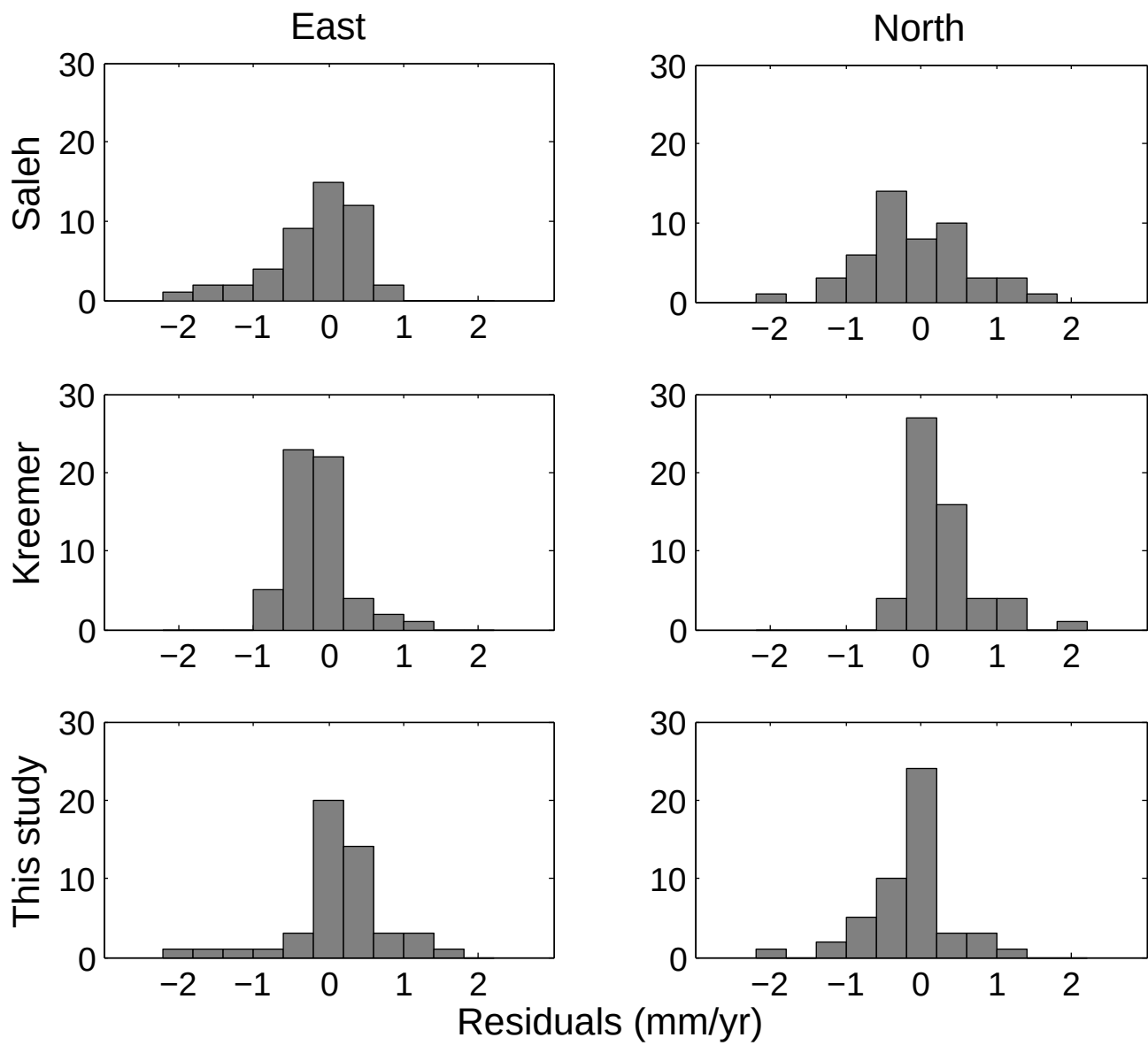
East
North
Saleh
Kreemer
This study
30
20
10
0
−2
−1
0
1
2
Residuals (mm/yr)

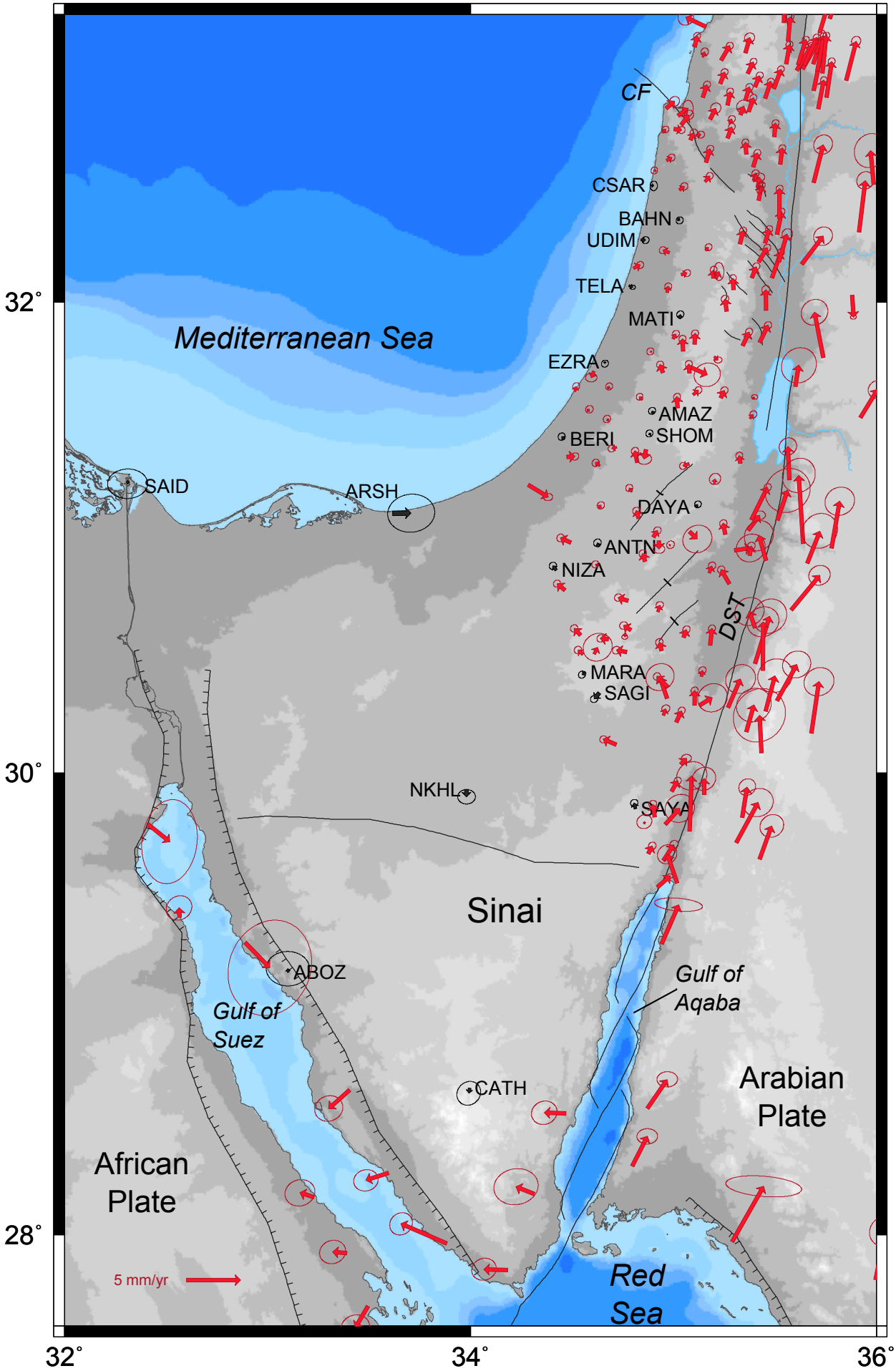
CF
CSAR
BAHN
UDIM
TELA
MATI
Mediterranean Sea
EZRA
AMAZ
SHOM
BERI
SAID
ARSH
DAYA
ANTN
NIZA
DST
MARA
SAGI
NKHL
SAYA
Sinai
ABOZ
Gulf of Aqaba
Gulf of Suez
CATH
Arabian Plate
African Plate
5 mm/yr
Red Sea
32˚
30˚
28˚
32˚
34˚
36˚

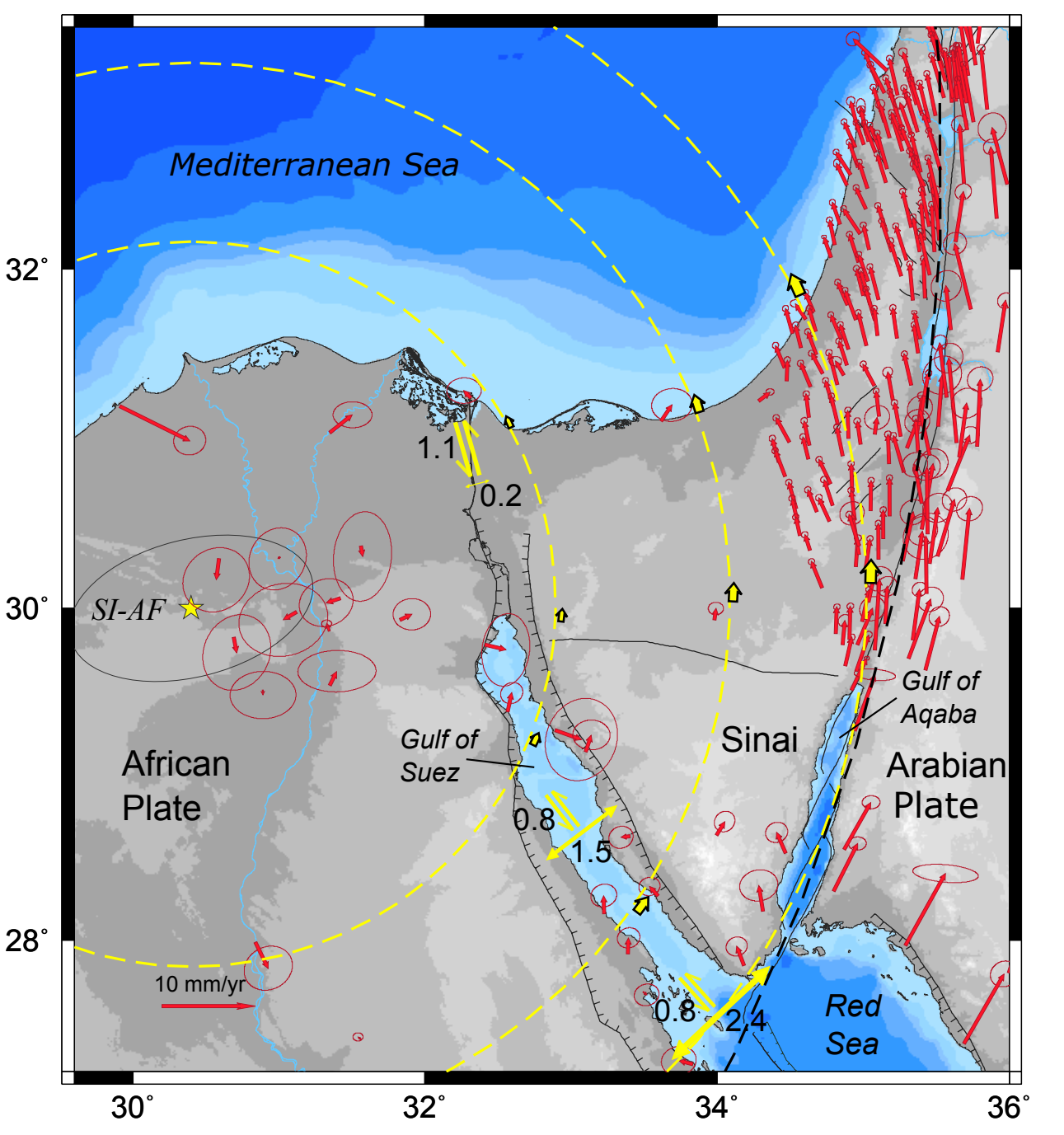
Mediterranean Sea
32˚
30˚
28˚
1.1
0.2
SI-AF
Gulf of Suez
Sinai
Gulf of Aqaba
African Plate
Arabian Plate
0.8
1.5
10 mm/yr
0.8
2.4
Red Sea
30˚
32˚
34˚
36˚

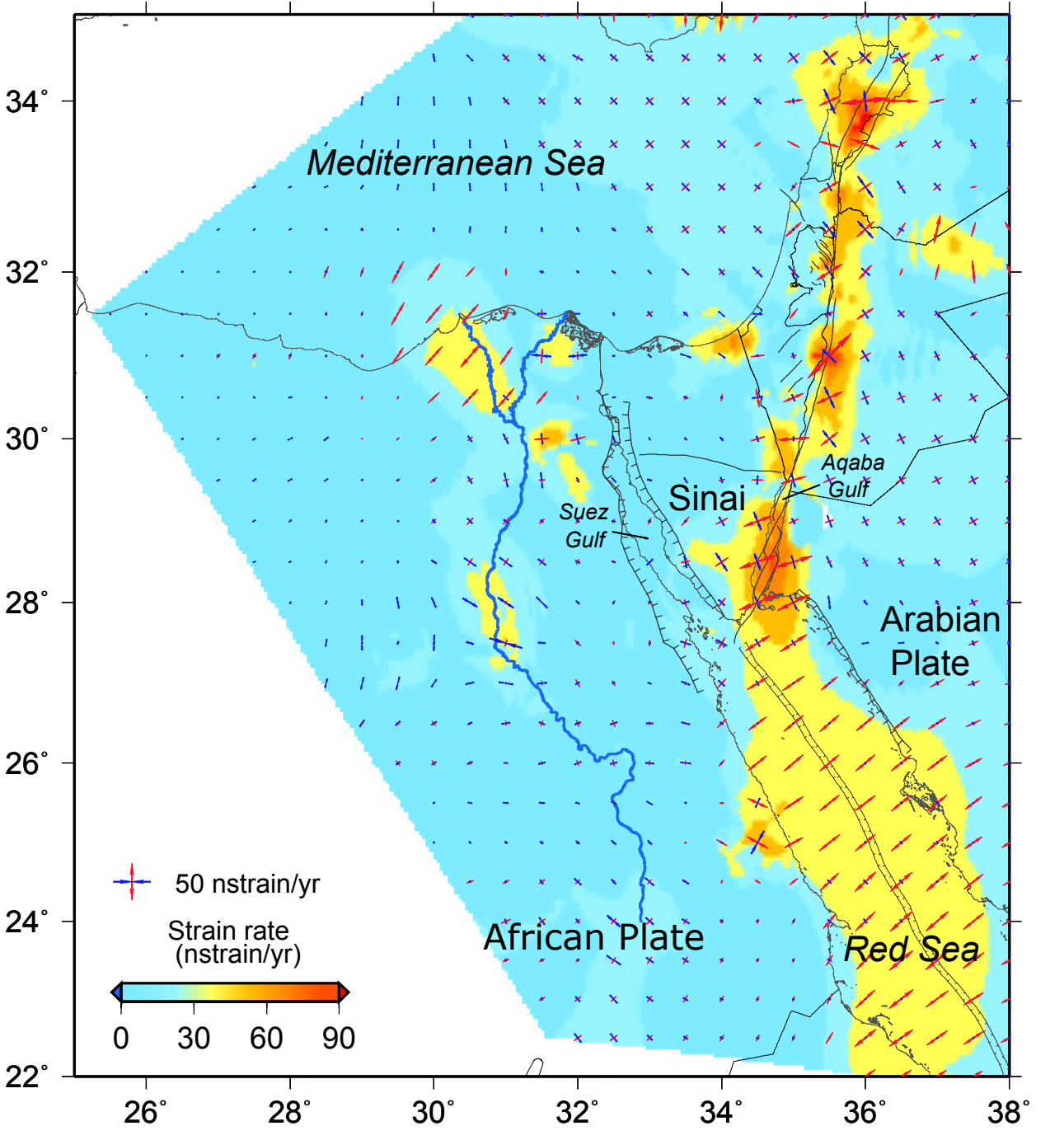
Mediterranean Sea
Sinai
Suez Gulf
Aqaba Gulf
Arabian Plate
African Plate
Red Sea
50 nstrain/yr
Strain rate (nstrain/yr)
0
30
60
90
34°
32°
30°
28°
26°
24°
22°
26°
28°
30°
32°
34°
36°
38°

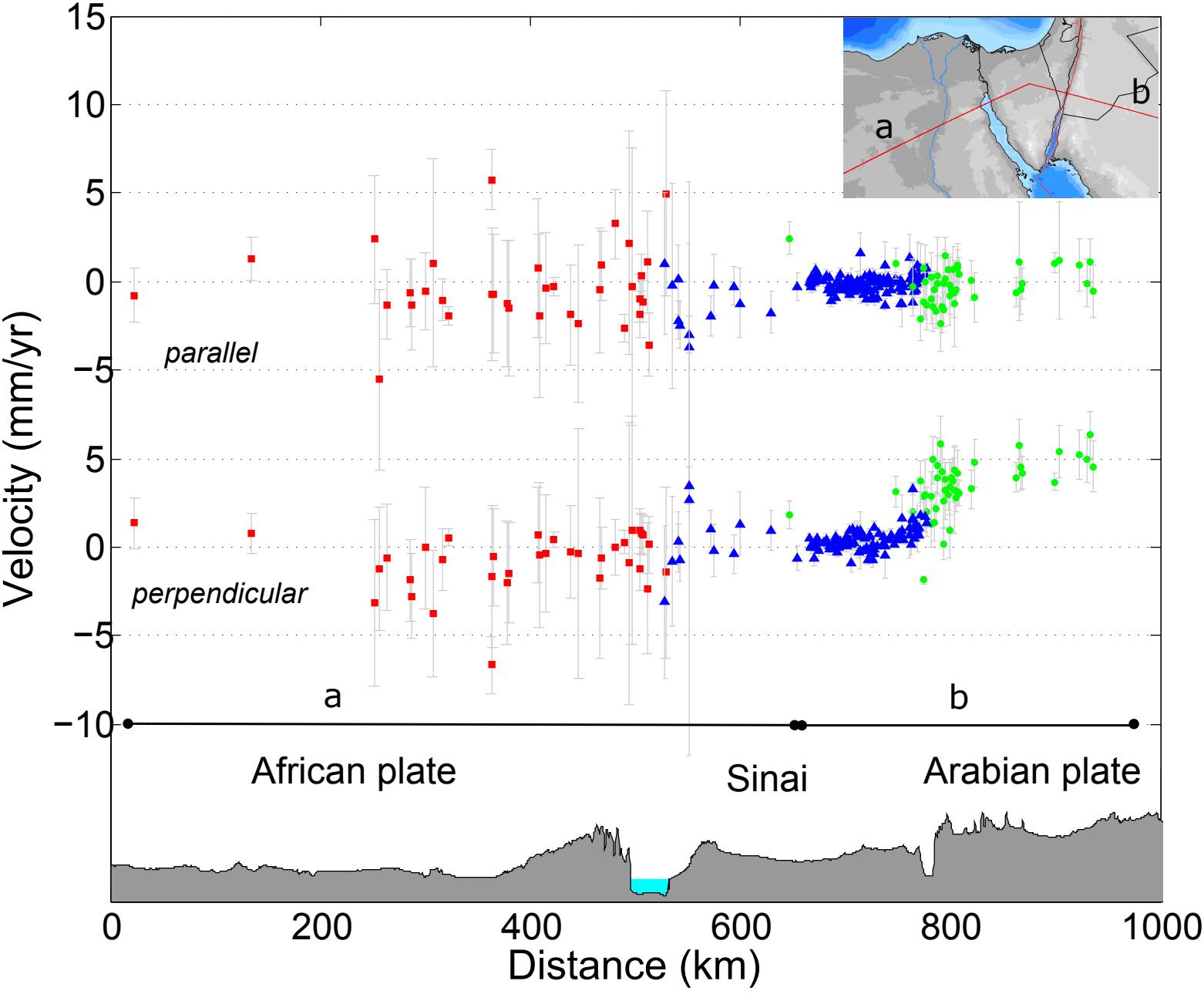
Velocity (mm/yr)
15
10
5
0
−5
5
0
−5
−10
parallel
perpendicular
a
b
African plate
Sinai
Arabian plate
0
200
400
600
800
1000
Distance (km)

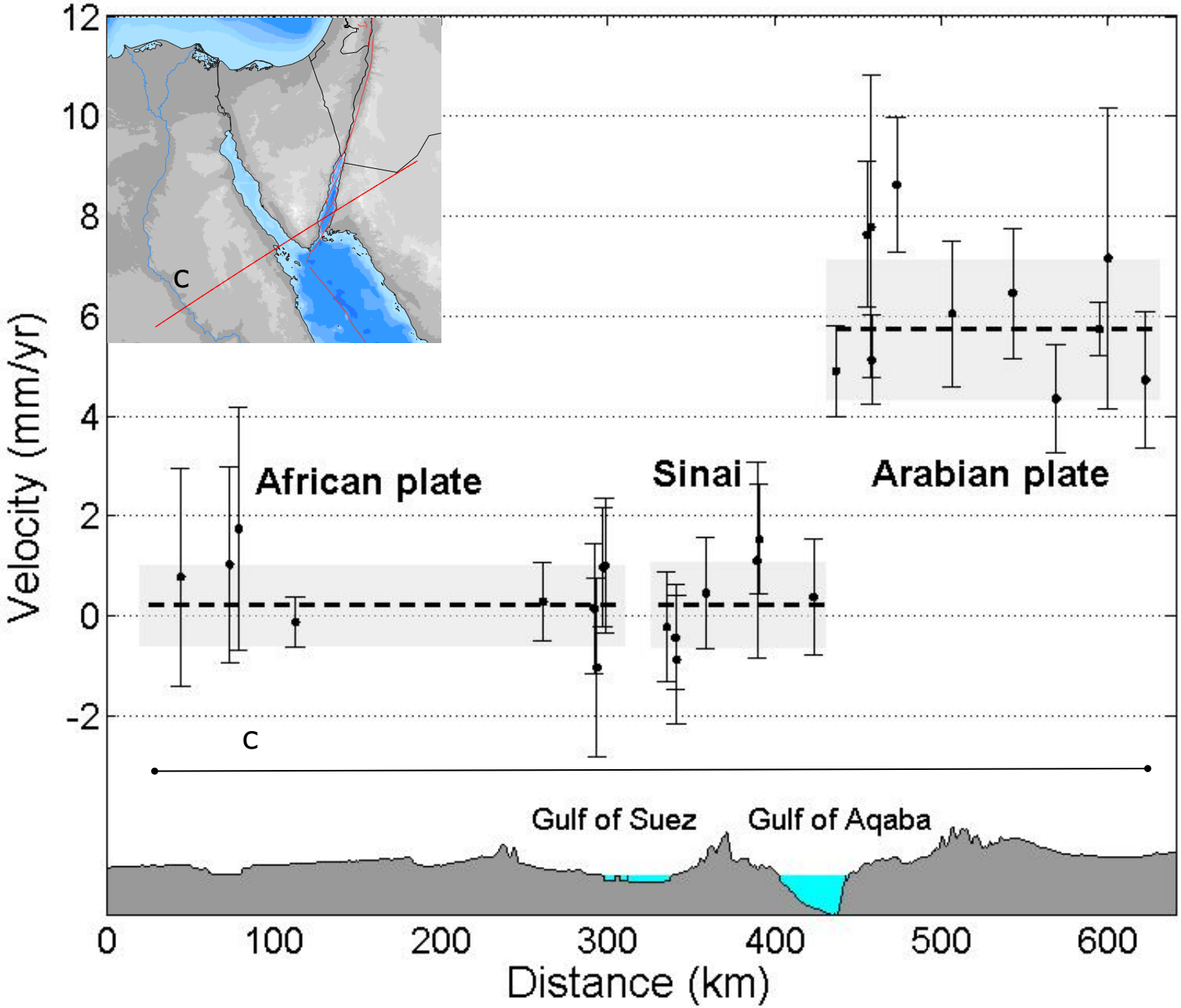
Velocity (mm/yr)
12
10
8
6
4
2
0
-2
C
C
African plate
Sinai
Arabian plate
Gulf of Suez
Gulf of Aqaba
0
100
200
300
400
500
600
Distance (km)

Supplementary Material

The content of this file consists in: three figures showing location, name and observation time span of each GPS station processed by Bernese software; one table with the IGb08 combined velocity field in East, North components.

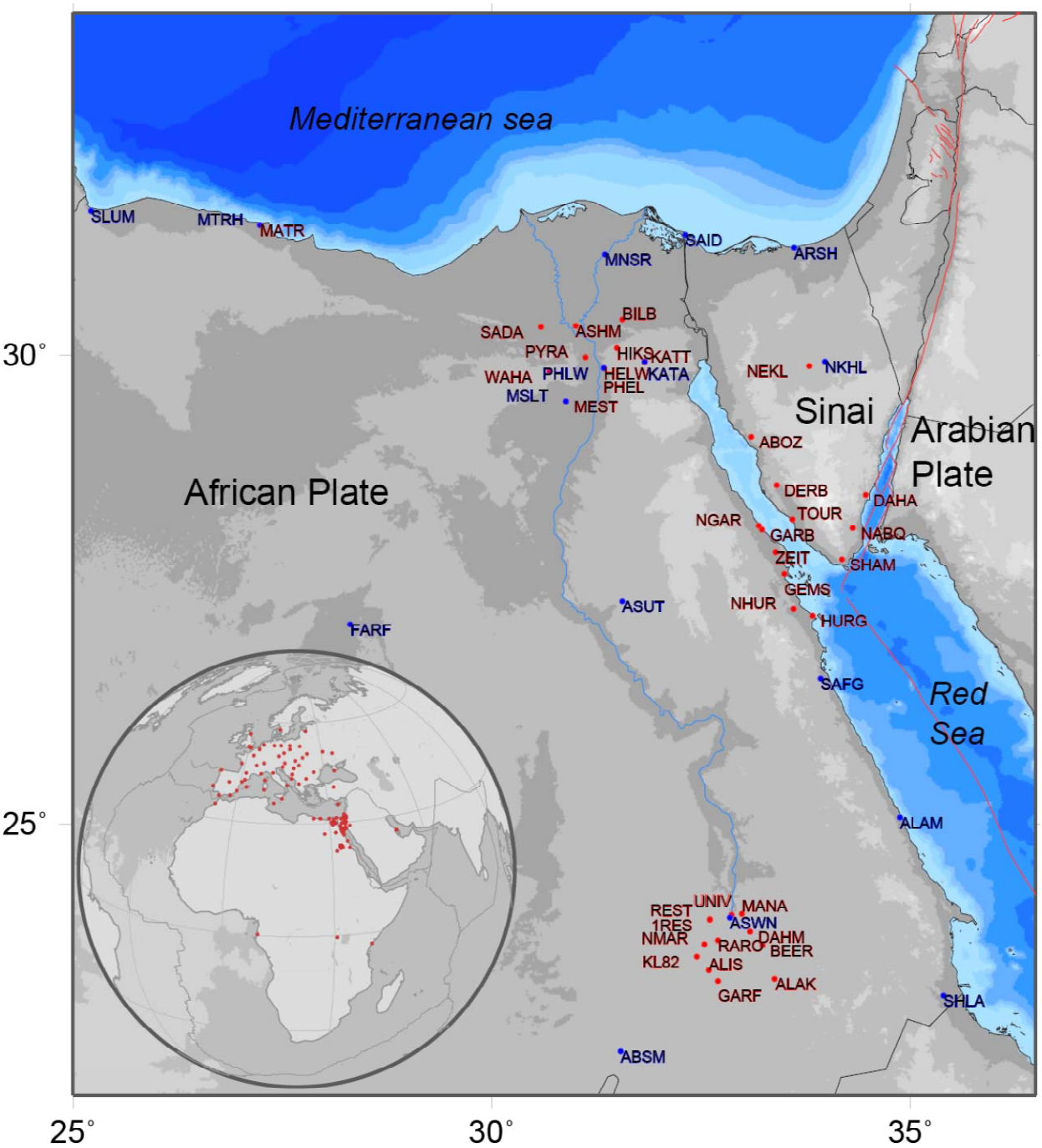

Figure S1: Map of permanent (blue) and non permanent (red) GPS sites processed by Bernese software in this work

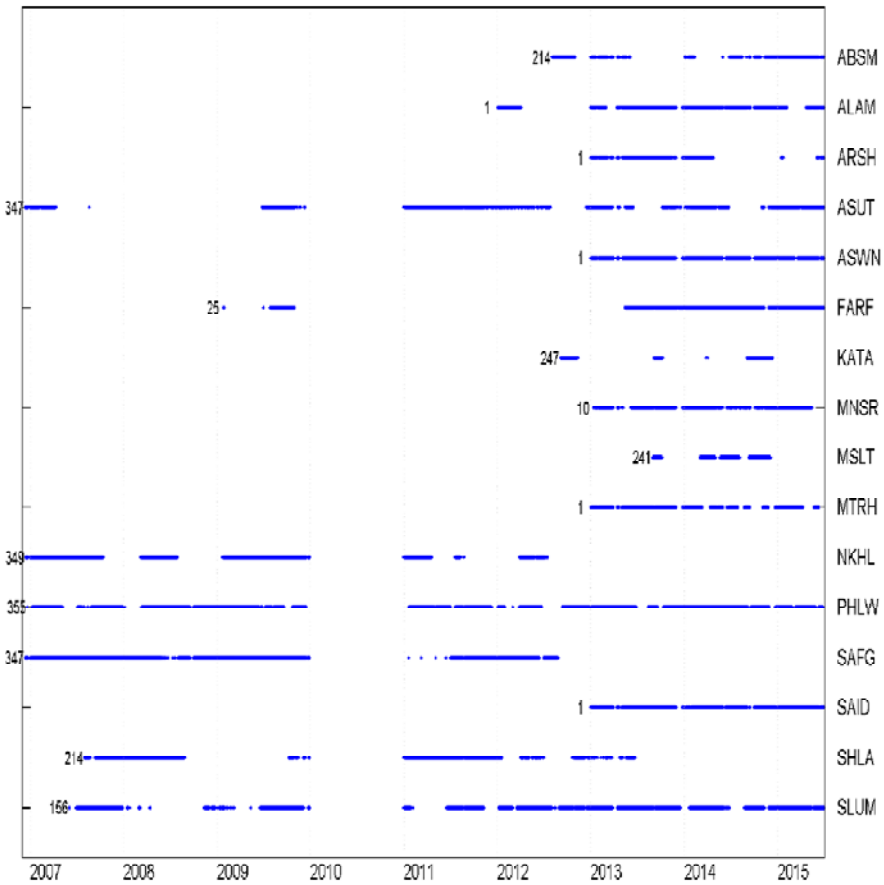

Figure S2: Observation time span of permanent GPS sites processed in this work; for each site the first observation DOY (Day Of the Year) is indicated.

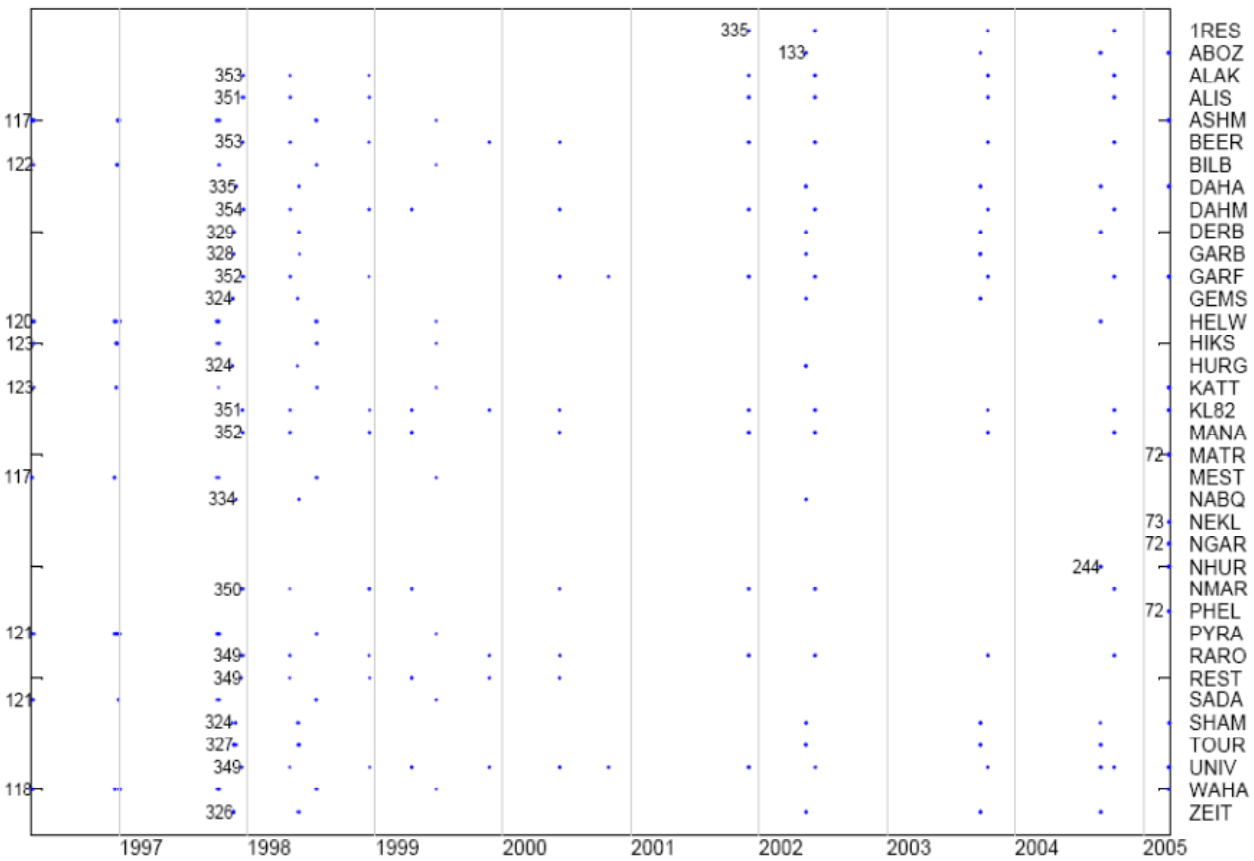

Figure S3: Observation epochs of non permanent GPS sites processed in this work; for each site the first observation DOY (Day Of the Year) is indicated.

Table S1: IGb08 combined velocity field in East, North components
(column 1: site longitude, column 2: site latitude, column 3: East component, column 4: North component, column 5: sigma of East component, column 6: sigma of North component, column 7: correlation between East and North components, column 8: site name)

lon	lat	VEast	VNorth	sigVE	sigVN	corrVE-VN	SiteID
°	°	mm/yr	mm/yr	mm/yr	mm/yr		
33.1024	29.1412	24.1186	19.5546	2.0583	1.6525	-0.0071	ABOZ
31.5438	22.4898	20.3584	18.6165	2.1346	1.5532	-0.0014	ABSM
33.3804	23.2943	23.1626	17.9054	2.1936	2.0486	-0.0039	ALAK
34.8777	25.0669	25.6043	18.2388	1.4099	1.1371	0.0329	ALAM
29.9110	31.1971	30.2645	14.3930	1.7558	1.5875	0.0490	ALEX
32.5933	23.3906	23.1444	17.6558	1.9860	2.0017	0.1124	ALIS
34.6066	31.7079	22.3771	19.2508	0.5406	0.4042	0.0145	ALON
33.6169	31.1075	24.5585	19.4424	2.2288	1.8223	0.0484	ARSH
31.0076	30.3020	22.8190	17.8291	3.2612	3.5292	0.1230	ASHM
31.5624	27.3968	23.1563	18.2032	0.5454	0.4444	0.0125	ASUT
32.8484	23.9708	24.4182	15.3161	1.8962	1.3981	0.0227	ASWN
33.2371	23.6644	23.0945	18.2951	3.0826	1.6631	-0.0021	BEER
34.4699	28.5288	22.8192	19.8348	1.2404	1.1410	0.0894	DAHA
33.0881	23.8187	23.9750	18.6210	1.9587	1.5052	0.0811	DAHM
33.4039	28.6306	22.6532	17.6293	1.3622	1.2454	0.0948	DERB
35.3921	31.5932	22.9818	20.2885	0.3006	0.2188	0.0011	DRAG
35.3688	31.0369	24.2713	21.5071	0.5410	0.4058	0.0132	DSEA
34.9206	29.5093	25.3939	20.9860	0.2731	0.2083	0.0254	ELAT
33.2283	28.1629	23.5858	19.6862	1.4482	1.2845	0.0905	GARB
32.7079	23.2706	23.1148	18.1578	1.5158	1.3149	0.1088	GARF
33.4943	27.6862	24.0915	17.4203	1.3797	1.2254	0.0888	GEMS
36.0999	29.1389	26.8161	23.5928	0.5761	0.4948	0.0501	HALY
31.3444	29.8619	22.9101	18.7672	0.5500	0.3958	0.0127	HELW
31.4964	30.0695	21.2800	17.1917	3.3281	8.1391	-0.0216	HIKS
33.8323	27.2444	22.3395	18.0713	1.9518	1.6306	0.0838	HURG
35.2024	31.7712	23.0111	19.7370	0.3684	0.2837	0.0234	JSLM
32.4529	23.5409	23.9861	17.7920	1.4543	1.0466	0.0598	KL82
34.8663	31.3778	22.7008	19.0650	0.6845	0.5139	0.0190	LHAV
32.9884	24.0151	24.8753	18.2905	1.7604	1.5729	0.1119	MANA
34.3139	28.1783	23.3527	20.3803	2.1465	1.7586	0.0794	NABQ
33.6060	27.3134	24.8438	20.1629	8.2696	5.9396	0.0082	NHUR
33.3964	35.1410	19.4743	15.1034	0.2559	0.1908	0.0001	NICO
33.9805	29.9294	23.7569	18.8995	0.8260	0.6821	0.0082	NKHL
32.5445	23.6780	23.7811	17.8152	2.2334	2.2134	0.1228	NMAR
35.0361	30.0384	24.3901	20.5562	0.4662	0.3567	0.0230	NRIF
31.1222	29.9757	21.7058	17.1527	5.0283	4.1410	0.0980	PYRA
34.7631	30.5976	23.3622	19.5367	0.2709	0.1987	0.0028	RAMO
32.7060	23.7189	23.7014	18.4819	2.5829	1.4235	0.0190	RARO

34.7966	28.2995	26.4162	22.6449	0.9701	0.7231	0.0208	RASH
32.6048	23.9517	24.8711	16.9023	3.4079	2.9133	0.0981	REST
30.5892	30.2934	22.7245	15.7954	3.7558	3.6373	0.1149	SADA
33.9291	26.5674	23.5874	18.6609	0.8428	0.6083	0.0177	SAFG
32.3143	31.2457	22.4503	18.6118	1.8680	1.3876	0.0177	SAID
34.1838	27.8464	23.0316	19.7108	1.1891	1.0715	0.0893	SHAM
35.3999	23.1068	23.1263	17.1933	0.9277	0.7412	0.0480	SHLA
34.2838	31.2282	24.7237	18.5798	0.4431	0.3432	0.0242	SLOM
34.8717	28.5515	26.6989	22.5996	0.9658	0.7188	0.0204	TAYS
34.7809	32.0680	22.7163	19.7575	0.2616	0.1996	0.0239	TELA
33.5964	28.2694	22.7646	18.7443	1.1824	1.0376	0.0845	TOUR
32.8685	24.0019	23.7972	18.2470	1.3218	1.1741	0.1061	UNIV
30.6921	29.8270	23.3919	16.3787	3.8628	4.2982	0.1241	WAHA
34.9283	30.9916	23.1845	19.1728	0.5420	0.4000	0.0144	YRCM
33.3914	27.9186	23.7412	19.4396	1.2607	1.1415	0.0930	ZEIT
39.1000	37.8630	18.4817	25.9189	1.0564	1.1839	0.0641	BUCK
36.3300	37.5720	16.9210	20.6842	0.5272	0.5341	0.0731	ANDR
34.8110	37.2070	12.2884	20.1037	0.4076	0.4140	0.0808	CAMA
35.8390	37.0550	15.0189	21.3722	0.5433	0.5514	0.0770	CEYH
34.6860	37.5250	11.0573	20.1326	0.4072	0.4139	0.0801	CFTH
35.3750	36.8200	11.5740	21.3780	0.5439	0.5519	0.0798	DKNT
34.1550	36.7180	13.5329	19.5521	0.3930	0.5868	0.0620	EREN
37.5740	36.9010	18.8017	25.3265	0.6026	0.5573	0.0637	GAZI
36.0730	37.3940	13.0565	21.5154	0.5150	0.8595	0.0304	KDRL
35.3400	36.5430	12.4834	23.2862	0.4084	0.4141	0.0809	KART
35.3690	37.5600	9.0394	19.7787	0.4069	0.4135	0.0772	KBSK
35.6850	37.3760	10.9858	22.1063	0.3923	0.5851	0.0559	KOZA
35.0760	37.2210	10.9208	23.0452	0.5433	0.5518	0.0796	KRHY
35.0180	36.8240	11.7312	20.9581	0.2594	0.4508	0.0328	SLCH
35.7950	36.8080	17.5240	18.6834	0.5275	0.7219	0.0691	YUMU
38.8170	23.4910	31.4189	26.9174	3.8100	1.0660	-0.2462	F005
37.3160	25.0580	30.0690	26.4441	3.2376	0.9015	-0.2610	F006
36.3150	26.5440	28.7328	26.6939	3.6838	1.0302	-0.2711	F007
35.2900	27.9690	28.2435	25.2211	3.7220	1.0417	-0.2805	F008
34.9410	29.2650	25.9598	23.5749	2.3580	0.6596	-0.2938	F009
36.1610	29.1430	27.5144	25.1463	3.7106	1.0642	-0.2879	F010
39.7830	24.5780	30.7293	27.6962	3.6074	1.0312	-0.2524	F012
42.9830	23.9510	31.2536	28.8917	2.9899	0.8744	-0.2384	F013
46.3970	21.8510	33.5214	29.7604	3.3106	0.9768	-0.2062	F019
46.6820	24.7440	31.6067	29.5129	2.2044	0.6677	-0.2254	F020
41.8080	27.7110	28.7816	28.4419	2.8894	0.8702	-0.2675	F024
43.8980	29.4090	27.5659	28.6672	3.6747	1.1576	-0.2642	F026
40.7380	31.0900	26.2054	27.1104	3.0126	0.9323	-0.2903	F027
43.5140	21.7950	33.2451	28.1175	2.7832	0.7973	-0.2218	F033
45.3540	26.5790	30.4421	29.3546	2.9600	0.9111	-0.2421	F039
45.5730	28.5270	29.1634	29.3569	3.2332	1.0215	-0.2504	F040
45.1830	21.9420	33.3027	29.8889	3.6264	1.0628	-0.2127	F077
35.0180	29.5280	23.3001	22.6329	0.9521	0.9414	0.1047	AQBA

37.6480	32.3330	24.5577	25.2477	0.8386	0.8583	0.0840	ASGF
36.8180	32.1560	23.3494	23.8770	0.7870	0.7873	0.0874	BISH
35.5800	30.6980	26.1128	23.4042	1.0519	0.9723	0.0921	DANA
35.6910	32.5010	23.1116	23.7533	0.9235	0.9434	0.0935	DASK
35.6590	30.8970	24.5309	23.2149	1.7400	1.7129	0.0964	DBUS
35.5720	31.2490	22.9518	23.3034	0.8609	0.8579	0.0967	DRAA
35.4560	30.9070	22.6661	22.4733	1.4266	1.4753	0.1007	FIFA
36.1890	32.1010	23.3732	24.2935	0.9218	1.0035	0.0866	HUGS
36.3680	30.6800	24.8541	24.5653	0.9312	0.9259	0.0937	JAFR
35.9150	32.2940	23.0024	25.1046	0.8410	0.8602	0.0931	JASH
35.9870	32.4930	22.0011	23.4841	1.5941	1.6737	0.0912	JUST
35.6320	32.1580	24.4470	22.8337	0.9288	0.9105	0.0924	MUD2
35.7180	31.0950	21.7912	20.9693	0.9912	0.9610	0.0943	MUTA
35.4030	30.4690	24.9621	24.5233	1.6702	1.6773	0.1006	NAML
35.4330	30.0860	23.7201	23.6445	2.5582	2.6291	0.1031	NAQB
35.7390	31.7660	21.9487	24.4650	1.3061	1.2675	0.0923	NEBO
35.6020	31.6440	23.1365	22.1841	1.7169	1.7323	0.0961	PANO
35.4690	30.3270	23.2310	21.3282	1.7284	1.6143	0.0921	PETA
35.4550	30.2650	24.6375	23.4539	1.7054	1.6552	0.0984	PETH
35.4030	30.6210	22.9806	21.6533	1.4404	1.3762	0.0964	QIRA
35.3400	29.8100	24.5135	22.9136	0.8246	0.8165	0.1020	QURA
35.1510	29.9070	23.9565	21.5139	1.1619	1.1325	0.1016	RAMA
35.9220	31.5140	24.5569	22.9347	0.9189	0.8800	0.0909	RSAS
35.4260	29.6300	25.3177	23.2242	1.1647	1.1154	0.0993	RUMM
35.5140	31.0780	24.1312	22.9528	2.2081	2.1601	0.0961	SAFI
36.5620	31.3190	23.9170	24.5068	0.8731	0.8705	0.0910	TUBA
35.3590	30.1760	24.5169	22.6145	1.7063	1.6555	0.0992	WADR
35.9220	33.7400	19.6155	23.7453	0.5960	0.6131	0.0886	ANJR
35.8800	33.8590	19.1467	24.1870	0.6057	0.5869	0.0849	HZRT
35.5790	33.5450	19.4409	22.1111	0.6369	0.6453	0.0902	JZIN
35.4010	33.6410	18.8613	22.3576	0.6926	0.7014	0.0907	JIYE
38.4370	33.5710	23.1650	27.6134	0.4254	0.4226	0.0745	KBDD
35.7610	33.5160	19.2738	23.5057	0.5711	0.5712	0.0887	MCHK
35.1620	33.1490	19.7928	20.9351	0.7743	0.8040	0.0947	RBDA
36.9130	32.7020	22.9471	26.5121	0.4250	0.4132	0.0832	RSHD
36.2850	33.5100	22.3524	23.9692	0.2350	0.2462	0.0886	UDMC
35.8800	32.0290	22.7366	18.3082	0.2830	0.2287	0.0703	AMMN
47.1230	37.3680	24.5584	22.7659	0.5240	0.5607	0.0357	KHOR
46.1620	36.9080	24.8783	23.6234	0.3281	0.3140	0.0301	MIAN
44.7500	37.5340	23.4669	25.2650	0.7889	0.8282	0.0422	BALA
47.0940	37.5760	25.9916	22.7015	0.9204	0.9523	0.0330	HSTD
46.0090	36.9300	22.4331	24.5551	1.8445	0.5746	-0.3456	MNDB
36.4670	34.1640	20.7248	25.1517	1.2947	1.2490	0.0806	ARSL
36.3790	34.4120	18.8687	23.4698	1.2588	1.1592	0.0765	HRML
36.1430	34.1840	20.4815	23.4766	1.1033	1.0561	0.0817	BRKA
35.0290	32.4700	22.5872	20.3120	0.3595	0.3601	0.0961	BRKA
36.0840	34.4510	19.6613	23.9966	1.0140	1.0222	0.0844	HABT
35.9090	34.4660	20.6380	22.7346	1.0690	1.0777	0.0852	ADAS

35.8290	34.0050	20.3604	22.5143	1.0690	1.0947	0.0879	FRYA
35.7670	34.0940	17.8193	20.5229	1.0687	1.0947	0.0879	HAYT
35.2700	30.2800	24.8737	22.7375	1.4687	1.4205	0.0992	ABK0
35.7800	30.9600	24.0908	24.6312	1.4513	1.3893	0.0933	AYN0
35.6400	30.9800	22.8883	26.5337	1.6184	1.6853	0.0998	BUR0
35.0800	29.7500	24.2652	25.1393	1.4766	1.3880	0.0994	JEM0
36.1900	30.2600	24.8891	24.9284	1.4880	1.3674	0.0889	JFR0
35.6800	30.1700	24.5786	25.0331	1.4723	1.3868	0.0947	MAN0
35.5100	30.3100	25.5780	23.5357	1.3862	1.3206	0.0964	QUL0
35.3100	29.7000	26.1671	23.8367	1.4763	1.3874	0.0981	ROM0
35.4400	30.4400	23.6790	24.6359	1.5549	1.4705	0.0958	SUL0
34.6100	30.5100	23.7668	20.4425	1.4292	1.3643	0.1014	BOR0
35.0800	31.0300	23.8806	19.3396	1.4249	1.3632	0.0972	DIM0
34.9700	30.3200	22.9700	21.9402	1.3876	1.3218	0.0997	MAP0
35.1300	30.2900	24.8717	20.7379	1.4571	1.3906	0.0989	MNH0
35.3000	30.9500	24.7840	20.3371	1.4248	1.3627	0.0961	TAM0
34.9600	29.7800	25.3639	21.4406	1.4468	1.3770	0.1012	TIM0
36.4970	35.5510	21.9608	24.8876	4.7226	5.0157	0.0808	AA04
36.4030	35.5470	23.9478	30.1809	4.4772	4.6380	0.0805	AA05
36.3710	35.5490	24.9818	21.7778	4.9595	4.4688	0.0711	AA06
36.1040	35.5980	19.7446	23.2786	1.1306	1.1462	0.0807	DOHA
36.0500	35.5950	23.3736	22.2379	2.3419	2.5538	0.0831	AA10
35.9910	35.5870	22.3361	25.0619	3.7006	3.8535	0.0823	AA11
35.8280	35.5810	21.1029	25.2224	3.1266	3.0333	0.0797	AA12
35.7860	35.6020	19.0565	21.8530	3.8651	3.8908	0.0819	AA13
36.6990	35.7890	23.7257	26.7464	3.0256	3.1905	0.0790	BB03
36.5640	35.9310	21.6880	23.4395	4.3927	4.2634	0.0751	BB05
36.5110	35.9740	25.3576	19.1036	3.1448	3.0737	0.0757	BB06
36.4210	36.0020	23.3239	21.4461	2.7012	2.8268	0.0792	BB08
37.2310	36.4410	21.7350	22.1740	3.3688	4.0062	0.0751	CC02
37.3290	36.0830	23.1995	23.7496	2.4558	2.8381	0.0765	CC03
36.3980	36.1750	22.8999	22.2817	2.8673	3.0886	0.0794	DD01
36.4730	36.1980	22.2093	22.0532	3.3024	3.5293	0.0788	DD02
36.6380	36.2160	26.2718	25.2319	2.7280	3.1149	0.0786	DD04
36.6960	36.2150	21.1520	21.3269	2.7653	3.1899	0.0783	DD05
36.7700	36.2300	23.4007	21.5885	2.7704	3.2884	0.0775	DD06
36.8660	36.2670	19.3827	23.8454	2.7747	3.0878	0.0776	DD07
36.9760	36.2700	21.4776	24.2775	2.8023	2.9676	0.0763	DD08
37.0700	36.2750	21.9614	20.3340	2.7819	2.7455	0.0727	DD09
37.3880	36.2940	21.7660	20.4842	3.5883	4.3766	0.0745	DD10
35.6850	36.9430	14.9268	18.0549	2.7250	3.0988	0.0792	PT01
35.6480	36.8570	16.1770	21.8944	2.5051	2.9129	0.0792	PT02
35.8660	36.9350	10.9040	23.5517	2.6539	2.9146	0.0788	PT04
35.9410	36.8960	14.6483	19.3835	2.3978	2.6360	0.0787	PT05
36.2690	36.1140	23.2757	24.0134	1.9479	2.1019	0.0801	PT07
36.1910	36.1660	23.3815	21.4325	1.8505	2.0222	0.0804	PT08
36.3410	36.0170	23.4512	21.5756	2.0874	2.3543	0.0805	PT09
36.0190	35.9410	20.7099	23.2840	1.9396	2.0558	0.0814	PT12

36.1010	36.2430	20.7131	22.0250	2.8049	2.9706	0.0800	PT26
36.2320	36.7410	16.6710	23.8626	5.3061	5.8615	0.0782	PT30
36.2570	36.6540	17.9707	21.8166	2.8377	3.0433	0.0781	PT31
36.3740	36.5350	20.1148	18.6866	2.5630	2.8011	0.0784	PT34
37.0090	36.8120	21.8901	27.0081	2.2166	2.4878	0.0751	PT35
36.9290	36.8950	20.4332	24.8989	1.9924	2.1869	0.0750	PT36
36.8290	36.9920	19.3427	19.1028	2.5618	2.7648	0.0748	PT37
36.7340	37.0090	19.1868	20.5775	2.5429	2.8013	0.0753	PT38
36.5980	37.1140	18.2711	21.2007	2.3417	2.8769	0.0732	PT39
36.5020	37.1580	18.6128	24.4845	2.4353	2.8230	0.0752	PT40
36.1790	37.1620	12.0557	25.1232	2.2379	2.4191	0.0767	PT43
35.5060	37.1620	13.1548	23.7401	2.3514	2.4981	0.0791	PT46
35.5990	37.0310	11.3482	19.8673	2.6029	2.8267	0.0794	PT47
42.4570	37.5280	19.6113	25.9106	3.9022	1.7476	-0.1610	SRNK
36.9740	36.2330	20.5610	25.4299	0.5577	0.5650	0.0748	HOWR
37.7160	36.2460	20.3512	25.8179	0.3831	0.4011	0.0730	KHBZ
38.4810	35.7820	21.5096	26.5904	0.5556	0.5810	0.0711	KRIN
38.7570	36.4610	20.7025	26.5407	0.5560	0.5641	0.0664	DBSS
40.5960	36.5840	21.1918	27.6404	0.5543	0.5638	0.0583	HMEH
40.7610	35.7540	22.3965	27.6753	0.5555	0.5642	0.0595	MRQD
46.4270	33.6480	25.3094	27.1151	1.1945	0.9764	0.0109	ILAM
40.6500	37.2460	19.5384	27.6190	0.9395	0.8687	0.0484	KIZ2
39.3360	37.6360	18.3400	27.4178	1.0553	1.2008	0.0641	AKTP
38.9970	37.1750	18.6675	26.3295	0.4421	0.4839	0.0663	HRRN
37.9020	37.2370	18.5250	25.9979	0.5417	0.5502	0.0678	ARGA
37.8860	37.5410	18.1368	25.0221	0.5972	0.5888	0.0653	CKRH
37.8690	34.6430	22.8428	27.0575	0.5737	0.5791	0.0753	JHAR
37.6340	35.8000	21.0463	25.5045	0.5426	0.5675	0.0747	AKIL
37.4360	37.5180	18.0118	23.9742	0.5416	0.5502	0.0689	ALAR
37.1060	36.6850	19.7003	24.4630	0.9197	0.9694	0.0742	KILI
36.9960	37.5220	15.8857	22.4135	0.5517	0.5971	0.0724	MRST
36.9720	37.1900	17.3409	23.6287	0.4204	0.4268	0.0718	SAKZ
36.9660	35.0490	22.3088	25.6123	0.5600	0.5656	0.0784	SALM
36.8810	35.6490	21.1547	25.0087	0.5608	0.5490	0.0751	KATR
36.7540	34.9140	21.1723	25.0757	0.7345	0.6508	0.0691	BLAN
36.6810	36.6640	19.1605	23.8987	0.5571	0.5649	0.0747	RAJO
36.6430	37.0880	16.9496	22.5064	0.6281	0.6011	0.0702	FEVZ
36.5780	35.4490	21.3521	24.9209	0.5595	0.5656	0.0790	KHAS
36.5730	34.9340	21.3291	24.9912	0.5586	0.5824	0.0821	TELF
36.5700	35.6380	21.0766	24.9324	0.5591	0.5655	0.0784	HASS
36.5500	34.0590	22.7341	24.8866	0.6564	0.6794	0.0848	MSHR
36.5240	36.7880	18.2791	22.7513	0.5318	0.5211	0.0732	HASA
36.5080	36.1460	19.8603	24.2639	0.5582	0.5653	0.0771	HARM
36.5030	34.9650	21.2780	24.2857	0.6015	0.6073	0.0808	HMRY
36.4650	36.5310	18.3031	24.0916	1.0927	0.9449	0.0635	ABAK
36.4190	35.1180	21.3476	23.8321	0.6189	0.5885	0.0769	DERS
36.4040	34.9480	22.4275	23.8663	0.5879	0.5936	0.0813	BARS
36.4000	33.8790	23.1977	24.6767	0.6157	0.6381	0.0861	ASAL

36.3430	34.9570	20.3388	23.9679	0.5606	0.5660	0.0816	BMRA
36.2700	35.2150	21.2119	23.6438	0.6031	0.5910	0.0794	DALY
36.2690	34.8850	21.0946	23.1432	0.5922	0.5611	0.0781	MSHT
36.2040	35.0900	21.3431	24.0955	0.5741	0.5798	0.0818	BNAB
36.1800	36.5400	16.4879	23.4895	0.9327	1.0009	0.0789	ISKE
36.1560	34.8820	21.1325	24.2455	0.5746	0.5800	0.0827	AJSH
36.1370	36.8990	14.5502	21.6471	0.4211	0.4273	0.0763	DORT
36.1310	36.0500	20.2617	22.1399	0.6989	0.6710	0.0761	SENK
36.1110	33.7810	22.8990	24.3755	0.6182	0.6218	0.0864	HOOR
36.1030	28.2680	26.7720	25.1215	1.3945	1.3342	0.0985	DUB3
36.0910	35.2470	20.9786	23.3987	0.5622	0.5497	0.0801	BATH
36.0510	33.6130	23.0941	24.7279	0.6441	0.6661	0.0886	SOBA
36.0330	34.9150	21.1650	23.2298	0.5609	0.5662	0.0832	HBAB
36.0100	33.6250	21.7568	24.4863	0.6206	0.6056	0.0855	ROZA
35.9960	27.8030	26.4697	24.8727	1.5507	1.5020	0.1015	DUB2
35.9540	34.8380	20.8106	22.9661	0.5611	0.5663	0.0838	MJDL
35.9400	36.4560	15.5639	21.6179	1.1376	1.0797	0.0749	ULUC
35.8700	36.3970	20.4596	22.1113	1.9853	2.0304	0.0794	ULCN
35.8310	27.4760	28.8167	26.0157	1.4266	1.3777	0.1031	DUB1
35.7690	35.6590	19.7065	23.2214	0.5869	0.5937	0.0820	RSHM
35.6910	27.3720	28.3449	24.9035	1.5585	1.4696	0.1019	DUB0
35.0890	31.7230	24.1364	19.3704	1.2906	1.1599	0.0894	BARG
33.9950	28.6390	24.5957	19.1032	1.1668	1.1676	0.1145	CATH
33.8830	27.9610	20.8913	21.3557	1.1163	1.0953	0.1158	KENS
33.3270	35.2230	19.0022	16.1355	0.1898	0.2109	0.0956	NEU1
32.5660	29.3790	23.8618	19.8596	1.2599	1.1997	0.1169	FANA
34.6810	30.5720	22.6714	19.9432	0.3626	0.3603	0.1039	ACRA
35.0220	31.5530	22.7059	21.0330	0.3470	0.3463	0.0990	ADRA
34.9010	31.5290	22.6646	20.2134	0.3471	0.3464	0.0998	AMAZ
35.2330	31.5960	23.1372	20.7623	0.3607	0.3600	0.0977	AMOS
35.7350	32.9560	22.2654	23.7511	0.3309	0.3320	0.0909	ANAM
34.6320	30.9670	23.0115	20.1838	0.3759	0.3742	0.1030	ANTN
35.2020	31.2330	23.1056	20.5118	0.5558	0.5538	0.0989	ARAD
35.1970	32.1000	22.4476	20.8422	0.3303	0.3490	0.0990	ARIL
35.5210	32.1680	23.1904	22.7623	0.5257	0.5259	0.0944	ARMN
35.0510	30.5800	23.7336	20.7437	0.3624	0.3601	0.1017	ARMS
34.9920	29.9210	24.4806	20.9730	0.3495	0.3462	0.1039	ARUT
34.5160	31.6240	22.7423	20.2626	0.3472	0.3466	0.1016	ASHK
35.7490	33.2620	21.8659	23.1401	0.3463	0.3294	0.0862	ATIV
34.9460	32.7080	22.2275	20.2616	0.3316	0.3324	0.0958	ATLT
34.9810	30.9720	23.2830	20.0326	0.3757	0.3740	0.1010	AVNO
35.4200	32.4260	22.5009	21.5318	0.3594	0.3598	0.0942	AVNR
35.3560	32.8410	22.2813	21.3825	0.3588	0.3598	0.0932	AVTL
35.2660	32.8230	22.1801	21.3518	0.3313	0.3322	0.0938	AZMN
35.0200	32.3490	22.4178	19.8319	0.3459	0.3462	0.0966	BAHN
34.9080	29.8120	23.8097	21.1340	0.3797	0.3575	0.1006	BERE
34.4630	31.4230	22.5207	19.9823	0.3454	0.3634	0.1051	BERI
34.4650	30.7810	22.5101	20.3833	0.3484	0.3466	0.1045	BERO

35.3670	32.9550	22.3710	21.2112	0.3311	0.3321	0.0928	BJAN
35.4520	32.2470	22.7404	21.4514	0.3458	0.3460	0.0946	BKOT
35.0480	31.7930	22.5560	21.1426	0.3467	0.3463	0.0981	BMIR
35.1380	30.4140	23.7029	20.5932	0.3626	0.3600	0.1017	BRAK
34.5420	30.5900	22.7999	20.4231	0.3626	0.3604	0.1046	BRNE
34.4750	31.3460	23.5911	19.8330	0.3615	0.3605	0.1027	BSOR
35.3410	31.8170	23.2582	21.3822	0.3445	0.3627	0.0992	CADM
35.3280	32.2430	22.6398	21.3426	0.3459	0.3461	0.0952	CBIR
34.9990	31.8460	22.8264	20.4224	0.3466	0.3463	0.0982	CNDA
35.0380	32.7410	22.6483	20.9110	0.4696	0.4708	0.0952	CPRK
35.1450	32.8550	22.2598	21.2213	0.3451	0.3461	0.0943	CSON
35.5270	32.5760	22.3320	21.6909	0.3474	0.3295	0.0894	CVDN
34.6770	31.6340	22.7837	20.0824	0.3471	0.3465	0.1007	CVEL
35.0970	31.6100	23.2458	20.4328	0.3469	0.3462	0.0984	CZUR
35.1090	31.1360	23.3150	20.2437	0.3337	0.3324	0.0998	DAYA
35.2360	33.0090	22.5705	21.4307	0.3449	0.3460	0.0933	ECOV
35.0390	32.1140	22.9164	20.1512	0.3462	0.3462	0.0972	ELKN
35.3930	32.5650	22.5216	21.4422	0.3454	0.3460	0.0939	ENRD
34.9800	32.2070	21.7067	20.2020	0.3461	0.3463	0.0972	EYAL
34.6620	31.7490	22.5933	19.6623	0.3469	0.3465	0.1004	EZRA
34.8040	32.1410	22.9260	20.2115	0.3463	0.3464	0.0984	GLIL
35.2300	32.9120	22.2706	21.1510	0.3471	0.3296	0.0901	GLON
35.6920	32.8840	22.7250	24.0210	0.3310	0.3320	0.0914	GMLA
34.8230	31.3230	22.6831	20.9822	0.3614	0.3603	0.1008	GORL
35.3870	32.1020	22.8695	21.1817	0.3460	0.3460	0.0954	GTIT
34.8480	31.5890	22.4544	20.1830	0.3332	0.3325	0.0999	GVRN
34.7960	31.1990	22.7418	20.2617	0.3477	0.3464	0.1013	HAIL
34.5530	30.5080	22.9998	20.2129	0.3628	0.3604	0.1048	HARI
34.9410	30.5240	23.3017	20.7329	0.3625	0.3601	0.1025	HDAV
35.4940	32.8920	22.5824	21.9604	0.3311	0.3321	0.0924	HKUK
35.4030	32.9000	22.3118	21.1809	0.3470	0.3296	0.0892	HZON
35.5550	32.9940	22.1733	22.0019	0.3468	0.3295	0.0881	HZOR
35.2770	30.8080	22.5853	21.4138	0.3619	0.3600	0.0998	IDAN
35.1820	32.7640	22.4494	21.0808	0.5109	0.5122	0.0943	KBIA
35.1590	32.2170	22.5972	20.3219	0.3460	0.3462	0.0962	KDUM
35.3780	31.5100	23.1793	20.5019	0.3469	0.3461	0.0972	KEDM
34.4950	30.9840	22.1301	20.2132	0.3600	0.3772	0.1063	KERN
34.9720	30.3680	22.6228	20.9628	0.3627	0.3601	0.1028	KIPA
35.6430	32.9880	23.0635	22.8109	0.3447	0.3458	0.0913	KNNE
35.6140	32.9900	22.5831	22.5719	0.3468	0.3295	0.0877	KNNW
35.6370	32.9740	23.2625	22.6812	0.3447	0.3458	0.0914	KNSE
35.6090	32.9680	23.2226	22.4809	0.3447	0.3459	0.0915	KNSW
35.0030	32.7240	22.6482	19.8821	0.3454	0.3462	0.0955	KRML
34.9650	32.8090	22.6377	20.6217	0.4833	0.4847	0.0953	KRMV
35.1110	32.6970	22.4396	20.0923	0.3612	0.3436	0.0915	KRTV
35.3970	32.5070	22.3207	20.8314	0.3593	0.3598	0.0941	LPDM
34.8610	30.9040	22.9925	20.6638	0.3620	0.3602	0.1019	MAAN
35.5110	32.2840	22.7713	22.2713	0.3319	0.3321	0.0942	MALS

35.1560	32.5040	22.5588	20.5713	0.3456	0.3461	0.0954	MAMI
34.9230	30.6900	23.5624	20.5635	0.3643	0.3437	0.0981	MAML
34.5660	30.4320	23.1897	19.5824	0.3489	0.3465	0.1050	MARA
35.0780	31.3180	22.3960	19.8228	0.3473	0.3462	0.0994	MASA
35.0320	31.9300	22.5565	20.3817	0.3465	0.3463	0.0978	MATI
35.4210	32.1680	23.2004	21.4617	0.3459	0.3460	0.0950	MCRA
35.1620	32.5840	22.4388	21.3110	0.3455	0.3461	0.0951	MDOZ
34.9140	32.5500	21.8965	19.9621	0.3318	0.3324	0.0965	MGAN
35.5450	33.1660	21.7836	22.3608	0.3307	0.3320	0.0913	MNAR
35.1040	30.2910	23.7030	21.3732	0.3488	0.3462	0.1022	MNHA
35.3590	32.6190	22.0013	21.2120	0.3315	0.3322	0.0939	MORE
35.5540	33.2300	21.6944	21.8919	0.3582	0.3597	0.0910	MRGL
35.0850	32.6780	22.2786	20.6805	0.3592	0.3600	0.0952	MRKA
35.4870	32.1020	23.2895	22.5313	0.3460	0.3460	0.0948	MSUA
35.3540	33.0390	22.1823	21.5418	0.4985	0.4817	0.0902	MTAT
35.3310	31.3190	22.8874	20.8435	0.3472	0.3461	0.0980	MZDA
34.7780	30.7370	22.3823	20.1826	0.3623	0.3603	0.1028	NAFA
35.3750	30.9290	23.4557	21.0128	0.3756	0.3737	0.0988	NECR
34.8290	31.0860	22.8635	20.6231	0.3617	0.3603	0.1015	NEGV
35.5640	33.0900	21.9936	22.4410	0.3742	0.3571	0.0880	NFTA
35.1040	33.0640	21.9597	21.0714	0.3469	0.3297	0.0903	NHRI
34.4230	30.8670	22.8495	20.1437	0.3623	0.3605	0.1045	NIZA
34.5760	31.5400	22.9014	19.9927	0.3750	0.3743	0.1015	NRAM
35.4560	31.9650	22.5508	22.0817	0.3858	0.4042	0.0978	NRAN
35.1040	31.8220	22.6560	21.0322	0.3466	0.3462	0.0977	NTAF
35.3710	32.7970	22.4011	21.3915	0.3313	0.3322	0.0933	NTFA
35.7540	32.8550	22.4744	23.6113	0.3448	0.3458	0.0911	NTUR
34.7700	30.5170	22.5007	20.0824	0.3766	0.3741	0.1035	ODED
34.6380	31.3090	22.4924	20.1234	0.3455	0.3632	0.1045	OFKM
35.2620	31.9610	22.3876	21.2311	0.3761	0.3574	0.0929	OFRA
35.8510	32.9260	22.8849	23.9514	0.4550	0.4564	0.0904	ORHA
34.7190	30.1210	22.5394	20.3839	0.3493	0.3464	0.1050	PARN
35.2560	31.0180	23.0160	21.1119	0.3616	0.3600	0.0993	PRES
35.7100	32.9630	22.4743	23.5412	0.3309	0.3320	0.0910	QZAB
34.7910	30.6110	22.7309	20.3331	0.3924	0.3715	0.0995	RAMN
34.7210	31.3870	22.3734	19.7727	0.3474	0.3465	0.1012	RHAT
34.9680	32.0390	22.5458	20.5426	0.3463	0.3463	0.0978	RNTS
34.6800	31.4990	22.6125	20.0328	0.3612	0.3604	0.1011	RUMA
35.4520	32.8510	22.4606	21.7110	0.3470	0.3295	0.0890	RVID
34.6340	30.3430	23.1097	19.2838	0.3651	0.3439	0.1008	SAGI
35.1770	30.8550	23.5551	20.7031	0.3758	0.3739	0.1002	SAIF
34.8140	29.8470	23.8200	20.4439	0.3657	0.3437	0.1010	SAYA
35.5230	32.3500	22.3217	22.9518	0.3477	0.3296	0.0900	SDLA
35.3850	31.0800	24.6776	23.1527	0.3614	0.3599	0.0984	SDOM
34.9660	32.5920	22.4973	20.2416	0.3456	0.3463	0.0961	SFIA
34.8590	29.7810	23.9673	20.1509	0.7352	0.6920	0.1009	SGUV
39.2620	21.5010	32.2873	27.8829	1.5632	1.4361	0.0818	SHAL
35.7210	33.1230	22.6747	23.2309	0.3307	0.3319	0.0905	SHAL

35.2960	32.0520	22.4185	21.1522	0.3462	0.3461	0.0960	SHLO
34.8880	31.4370	22.7247	20.1431	0.3473	0.3464	0.1001	SHOM
34.9520	29.6250	25.0900	21.4232	0.4059	0.4016	0.1049	SHOR
34.6250	30.8860	23.0007	19.9533	0.3482	0.3465	0.1033	SHVT
35.0800	31.7000	22.6063	20.8731	0.3468	0.3462	0.0983	SNSN
34.8920	31.7890	22.4850	20.0020	0.3467	0.3464	0.0990	TLSR
34.8410	32.2600	22.6558	19.9020	0.3461	0.3464	0.0978	UDIM
34.8770	29.6540	24.4495	20.6434	0.3779	0.3739	0.1053	UZIA
35.4250	31.8290	23.4399	21.7521	0.3603	0.3599	0.0960	VERD
35.2670	32.6860	22.4097	21.1307	0.3315	0.3322	0.0942	YAFI
34.9010	31.0070	23.5331	20.5537	0.3618	0.3602	0.1013	YERU
35.7140	32.8080	22.5241	22.9215	0.3173	0.3182	0.0915	YOAV
35.4980	32.6910	22.1624	21.4417	0.3472	0.3295	0.0892	YVEL
34.9490	31.7030	22.3948	20.7026	0.3468	0.3463	0.0990	ZACH
34.9510	30.2470	23.9121	20.5831	0.3929	0.3714	0.0994	ZHOR
35.0150	30.2190	24.2117	21.0332	0.3490	0.3462	0.1029	ZIHA
34.6300	31.1290	23.2513	20.1131	0.3618	0.3604	0.1025	ZLIM
35.1810	30.5470	23.6954	21.6034	0.3484	0.3462	0.1011	ZOFR
35.2760	32.7460	22.1999	20.5108	0.3452	0.3461	0.0940	ZPRI
30.8900	29.5100	23.1703	17.4790	3.5509	2.5619	0.0086	MSLT
47.4290	32.6920	26.0029	26.3039	2.0622	2.0891	0.0359	DELO
47.7390	33.0570	23.9083	26.7804	2.0321	2.0623	0.0345	GORI
48.1750	33.4060	26.6860	26.4040	2.0151	2.0498	0.0327	KORA
36.3780	26.4580	28.5636	25.1748	0.5901	0.4641	0.0741	ALWJ
35.0230	32.7790	22.8217	20.6641	0.5097	0.7995	0.0060	BSHM
34.8900	32.4880	22.3391	19.8996	0.3598	0.4767	0.0523	CSAR
38.9710	21.9490	32.0442	27.1776	0.6784	0.6564	0.0904	DORH
35.7710	33.1820	22.6664	22.9167	0.4319	0.2935	0.0363	ELRO
48.0870	29.0830	28.2296	30.0774	1.0096	0.6970	-0.0204	FG40
35.4160	32.4790	22.3471	21.1006	0.5205	0.4196	0.0718	GILB
35.4200	32.4800	22.2702	19.9402	0.2611	0.3766	0.0884	GILB
35.7850	33.3080	24.0428	21.8276	0.9165	0.8859	0.0860	HRMN
38.8180	37.1920	17.6036	25.9862	1.4411	1.2583	0.0506	HRR0
47.7960	30.4870	26.4327	29.7387	0.8644	0.7851	0.0241	ISB0
44.0110	36.1600	23.0444	29.2500	0.7971	0.7918	0.0431	ISER
45.8080	32.5020	23.2264	26.1209	0.8149	0.8213	0.0425	ISKU
44.3530	32.0130	25.6008	28.1678	0.7923	0.6161	0.0135	ISNA
43.6730	34.6010	24.8273	30.3412	1.2931	1.2098	0.0409	ISSD
35.1450	33.0230	21.9297	20.5080	0.3697	0.3872	0.0480	KABR
35.6890	32.9950	22.6933	22.7980	0.3790	0.6023	0.0064	KATZ
39.3360	22.1550	31.6630	26.0396	0.8286	0.6644	0.0604	KHLS
47.9710	29.3250	29.3065	30.2136	0.5404	0.4595	0.0154	KUWT
35.6740	34.1150	21.7493	21.8950	1.1006	0.8383	0.0567	LAUG
35.3310	32.7820	22.2805	20.9037	0.7287	0.6479	0.0838	NZRT
46.4010	24.9110	31.7080	29.3972	0.5548	0.5218	0.0389	SOLA
39.1130	22.2760	32.2646	27.5779	1.5930	1.6850	0.0990	THW0
34.6600	25.5000	28.6803	21.8900	3.3888	2.3048	-0.0000	AD01
34.5400	25.4400	24.9803	19.4801	2.0509	2.3943	0.0000	AD02

34.5000	25.3600	22.6704	18.4402	3.1229	1.7288	0.0142	AD03
34.3800	25.3600	21.4903	18.5302	2.8238	2.6720	0.1158	AD04
34.4200	25.2300	25.1404	19.3402	2.3579	2.0448	0.1056	AD05
34.5000	25.2400	22.2703	20.4002	2.8822	2.7950	0.1177	AD06
34.6200	25.2400	23.7703	19.2403	1.9945	2.5176	0.1312	AD07
34.7500	25.2900	25.5404	18.1302	2.7150	2.6621	0.1169	AD08
34.6900	25.4100	24.3603	18.5403	1.6306	3.4475	0.0885	AD09
34.6300	25.3300	23.0303	17.5002	2.0848	2.2070	0.1238	AD10
34.4800	25.3100	23.6903	18.5303	1.4055	2.6902	0.1055	AD11
30.5600	27.8700	20.2004	14.6501	5.8298	2.9351	0.0198	ARAB
29.5700	30.8600	21.7302	16.6602	1.0242	1.9823	0.0629	BORG
28.9600	24.3200	22.5002	19.9003	3.4063	6.4644	0.1293	DKHL
31.3500	29.5400	23.9604	19.4502	4.4421	2.3580	0.0220	ELSF
32.3300	30.2800	28.3204	19.7802	6.4230	4.7341	0.0860	FAYD
31.3600	26.5400	24.8002	17.3903	1.6368	3.4095	0.0868	GHNA
31.4200	30.0600	21.6703	17.4602	3.0616	2.7202	0.1169	HYKS
44.4400	33.3400	24.5327	26.7159	1.1242	0.7901	-0.0114	ISBA
31.8300	29.9300	24.5043	18.5079	2.0249	1.7207	0.0142	KATA
32.8900	29.2700	26.3103	16.7902	4.1076	4.6802	0.1233	KENT
31.3500	31.0400	25.4547	19.8713	2.1166	1.4061	-0.0031	MNSO
32.3300	25.6800	29.0204	15.9801	6.7943	2.5499	-0.0946	NAGH
31.5600	30.3700	23.3538	16.8031	3.3058	5.0843	0.0857	PLBS
31.0100	26.9400	28.9003	16.5402	3.3834	5.3158	0.1280	PORT
32.6000	30.2500	18.8102	19.7802	7.4473	16.5978	0.0314	QANT
32.8900	26.1800	25.4703	17.1601	4.3394	2.5899	0.0468	QENA
32.6900	29.7700	23.7902	18.2401	6.6776	2.8005	-0.0749	SEDR
30.8400	27.9900	24.6702	15.2201	2.7467	2.5078	0.1300	SHAD
31.8200	26.4700	25.3302	18.4202	1.6915	3.9710	0.0596	SOHG
32.4100	29.7800	25.6002	17.3202	2.7284	4.1263	0.1087	SOKN
31.3500	27.0400	25.6002	16.5301	1.8276	2.5496	0.1360	WADI
35.2100	32.1000	22.6997	20.6828	0.4890	0.8828	-0.0160	YOSH
32.8100	28.7100	26.7902	19.2202	6.0726	8.8475	0.1176	ZAFR
27.2310	31.3460	22.4625	17.9527	1.3328	1.1852	0.1335	MATR
25.2122	31.4914	22.1028	18.4378	0.6094	0.4715	0.0345	SLUM
28.3104	27.1485	23.5785	18.0425	1.6116	1.4892	0.1307	FARF